Correcting dispersion corrections with density-corrected DFT

Minhyeok Lee[a], Byeongjae Kim[a], Mingyu Sim[a],
Mihira Sogal[b],Youngsam Kim[a], Hayoung Yu[a],
Kieron Burke[b], and Eunji Sim[a*]

[a]Department of Chemistry, Yonsei University, 50 Yonsei-ro Seodaemun-gu, Seoul 03722, Korea
[b]Department of Chemistry, University of California, Irvine, CA 92697, USA

May 7, 2024

Almost all empirical parameterizations of dispersion corrections in DFT use only energy errors, thereby mixing functional and density-driven errors. We introduce density and dispersion corrected DFT (D^2C-DFT), a dual-calibration approach that accounts for density delocalization errors when parametrizing dispersion interactions. We simply exclude density-sensitive reactions from the training data. We find a significant reduction in both errors and variation among several semilocal functionals and their global hybrids when tailored dispersion corrections are employed with Hartree-Fock densities.

dual-calibrated DFT | density functional theory | density-corrected DFT | dispersion corrections | delocalization errors

Significance

Density functional theory (DFT) is widely used in chemistry. Still, even the most popular approximations suffer from two fundamental limitations - they often predict that electrons are more delocalized than they should be and fail to capture weak long-range attractions between molecules. These issues are usually addressed separately by density correction schemes and empirical dispersion corrections. Here, we show that a "dual-calibration" approach, fitting dispersion corrections on density-corrected DFT energies, provides a more balanced and robust solution. The resulting density and dispersion-corrected DFT method improves accuracy across various functionals and chemical systems, particularly those susceptible to density delocalization errors, by simultaneously addressing two major error sources in DFT.

Introduction

Kohn-Sham density functional theory (KS-DFT)[1,2] is a standard method in computational chemistry, striking a balance between computational efficiency and accuracy.[3] However, the quality of results depends on the quality of the approximate exchange-correlation functional used.[4] Density-corrected DFT (DC-DFT) is a generic methodology for separating errors in the functional from errors in the self-consistent density.[5,6] The principles of DC-DFT follow directly from simple (functional) analysis and can be applied (in principle) to every approximate KS-DFT calculation ever run. In practice, for DC-DFT to yield improved energetics in (a subset of) KS calculations, several conditions must be met.[7] In some cases, these conditions can be checked with highly accurate quantum chemical calculations[8,9], while in others, improved energetics resulting from the procedure suggest the conditions have been met. In either case, DC-DFT has had an impact in a variety of challenging areas for standard DFT calculations.[10–24]

Semilocal density functional approximations (DFAs) often fail to capture long-range dispersion interactions accurately due to their local nature.[25] To remedy this, many dispersion corrections have been developed as empirical pair-wise additions to DFT energies, with parameters fitted to databases dominated by weak interactions.[26–31] These corrections are computed for each XC functional and then tested on other databases where dispersion effects vary in magnitude. However, in all these databases, the energy error of the DFA mixes both functional and density-driven errors, which in turn affects the choice of optimum dispersion parameters. This effect is particularly acute for reactions that are density-sensitive, i.e., those whose density-driven errors are large. In some cases, density-driven errors are much larger than dispersion corrections and can hopelessly distort the choice of dispersion parameters.[32]

The remedy is very simple. Drop any density-sensitive reactions from the training data, find the optimal dispersion parameters, and then test on all the data using Hartree-Fock (HF) densities. It is known that HF densities typically greatly reduce density-driven errors for density-sensitive reactions and do little (if any) harm for insensitive cases.[5]

To fully assess the impact of both dispersion and density corrections, we apply them to a wide range of XC approximations, aiming to demonstrate the generality of the improvements and the reduction in the variance of predictions across different functionals. Figure 1 illustrates our results, using the extensive GMTKN55 database for general-main group thermochemistry, kinetics, and non-covalent interactions[33]. The left panel takes several popular semilocal XC approximations, showing their improvements upon first

*esim@yonsei.ac.kr

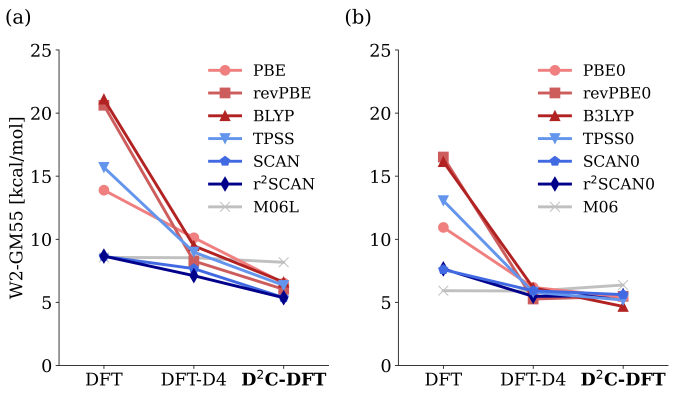

Figure 1: Performance of DFT, DFT-D4, and density and dispersion corrected DFT (D^{2}C-DFT) for several semilocal functionals (a) and their corresponding hybrids (b), measured by the weighted total mean absolute deviation on the GMTKN55 database[33] (W2-GM55). D^{2}C-DFT significantly enhances accuracy and reduces variability across a wide range of functionals. M06 and M06L show no such improvement.

adding dispersion corrections without DC-DFT analysis (the standard approach, DFT-D4) and then adding density corrections using the principles of DC-DFT (D^{2}C-DFT). All but one of the functionals improve significantly with each correction. Moreover, their errors become comparable once both corrections are employed. The glaring exception is M06L. Because of its highly empirical construction, which likely mixes functional and density-driven errors and already includes dispersion, it shows no improvement whatsoever, moving it from among the best performers without correction to the worst after correction. We also point to the right panel, which are global hybrids made from those on the left, where all the same effects occur, but less dramatically, because a fraction of the HF density is already being used.

The current paper presents an example of what we call dual-calibration, a general approach in which empirical parameters in a DFT correction are chosen under DC-DFT principles. Dual-calibration aims to resolve density-driven and functional errors simultaneously, with the specific combination of density correction and dispersion correction being one such example. It was first used to create the BL1p functional[32] and later to create the HF-r^{2}SCAN-DC4 method[21]. The latter, which employs an explicit dispersion formula, has shown remarkable accuracy across various applications, from water complexes to biomolecules, and has been further refined.[34] By studying many different DFAs, the present work demonstrates that D^{2}C-DFT is a general procedure that should be adopted whenever empirical parameters are optimized in DFT calculations.

Background

Density-Corrected DFT

DC-DFT provides a framework for analyzing the energy error in *any* self-consistent KS-DFT calculation.[5,11] The energy error can be separated into the contribution due to errors in the functional (for a given density, n) and those in the self-consistent density ($\tilde{n}$, introduced by the use of an approximate XC potential). Using tildes for approximate quantities, we write:

$$\begin{aligned}\Delta E &= \tilde{E}[\tilde{n}] - E[n] \\ &= \underbrace{\tilde{E}[\tilde{n}] - \tilde{E}[n]}_{\substack{\text{density-driven} \\ \text{error}(\Delta E_D)}} + \underbrace{\tilde{E}[n] - E[n]}_{\substack{\text{functional} \\ \text{error}(\Delta E_F)}}\end{aligned} \tag{1}$$

The errors in most KS-DFT calculations are dominated by the functional contribution, but even very small density-driven errors can have an impact on overall performance, as we show below.

For theoretical studies of small molecules, accurate densities are sometimes available from quantum chemical methods, such as Coupled Cluster Singles and Doubles (CCSD)[8]. However, most practical applications use the HF density as a proxy for the exact one, as its computational cost is often comparable to the corresponding KS-DFT calculation. For cases where density-driven errors are significant, the HF density is usually a good proxy. In such cases, a useful indicator is the 'density sensitivity,' defined as,

$$\tilde{S} = |\tilde{E}[n^{\mathrm{HF}}] - \tilde{E}[n^{\mathrm{LDA}}]|. \tag{2}$$

This density sensitivity, which makes use of HF and LDA densities, provides a crude measure of how sensitive the density in a system is likely to be to the choice of XC functional. If the sensitivity is low, the density-driven error is small in the system. Conversely, if the sensitivity is high, there is a higher probability of significant density-driven error in the system.[35] We have shown that significant density sensitivity suggests that a system is suffering substantial density-driven error, which can be mitigated by employing HF density. In cases where the HF density is a good proxy for the exact density, we expect

$$D[n^{\mathrm{HF}}] = \tilde{E}[n^{\mathrm{HF}}] - \tilde{E}[n] \tag{3}$$

to be smaller than the density-driven error of the usual calculation. While it can make sense to vary the cut-off for different-sized systems or weaker bonds or define in a new way,[36,37] here, we simply apply 2 kcal/mol to all cases.

Likewise, it has been shown that ROHF (restricted open-shell) can perform better than UHF (unrestricted) for DC-DFT calculations.[38] Here, for ease of implementation and to keep computational costs down, we use UHF throughout whenever HF breaks symmetry.

Dispersion-Corrected DFT

Since it is widely acknowledged that (semi)local DFT cannot correctly capture long-range dispersion interaction,[25] various methods to correct dispersion interaction have been developed. These include explicit nonlocal density functionals[39–41], empirical functionals[42,43], and additive correction methods[26–31]. Nonlocal methods are often computationally expensive in codes using atom-centered basis sets, and empirical functionals are known to miss capturing accurate asymptotic behavior.[44]

Considering the cost-accuracy balance, which is also the philosophy of DFT, the practical choice is additive correction. In Grimme and coworkers' additive dispersion model, DFT-D4[26,27], dispersion energy is defined as,

$$E_{\text{disp}}^{\text{D4}} = \underbrace{-\sum_{AB}\sum_{n}^{6,8} s_n \frac{C_n^{AB}}{R_{AB}^n} f_{\text{damp}}^n(R_{AB})}_{E^{(2)}} + E^{(3)}, \qquad (4)$$

where the sums are over all atom pairs A and B separated by R_{AB}, and the D4 model swiftly evaluates two-body ($E^{(2)}$) and three-body ($E^{(3)}$), contributions to the energy based on dispersion coefficients (C_n^{AB}) between atoms using fractional coordination numbers and atomic charges from a structure.

Additive corrections require appropriately fitted global parameters for each functional since the base energy from DFA already contains varying degrees of intermediate-range dispersion depending on the functional used.[45] In its major two-body term, there are global parameters s_6 and s_8, which directly scale the multipolar contributions (dipole-dipole and dipole-quadrupole interactions, respectively), with $s_6 = 1$ unless it is paired with double-hybrid functionals. In contrast, s_8 is specifically tuned to the functional in use, adjusting the contribution of medium-range dispersion.[46]

Further, the D4 model employs the Becke-Johnson choice of damping function[47] to prevent the dispersion energy from diverging at small interatomic separations:

$$f_{\text{damp}}^n(R_{AB}) = \frac{1}{1 + (R_1^{AB}/R_{AB})^n}, \qquad (5)$$

where $R_1^{AB} = a_1 R_0^{AB} + a_2$ is a scaled and offset Van der Waals radius R_0^{AB}. The parameters a_1 and a_2 are globally chosen for a given functional.

The fitting of these parameters s_8, a_1, and a_2 is a critical process in dispersion-corrected DFT. They need to be optimized to reflect the unique dispersion characteristics of different functionals without double-counting the dispersion effects already included in the base functional. Typically, the optimization process minimizes the discrepancy between calculated and reference interaction energies, leveraging databases rich in non-covalent interactions for effective parameterization.[48] Details on the DFT-D4 can be found in Ref. [26].

Functionals, Datasets, Basis sets, and Methods Used

Our study involves many standard (and some non-standard) choices of DFA, chemical databases, basis sets, and methodologies. In this section, we explain these choices.

Functionals: We include 7 popular semilocal functionals; 6 with few or no parameters, plus one heavily parametrized example. The 6 account for most DFT calculations at present and are computationally efficient for both molecules and materials. There are 3 generalized gradient approximations (GGAs) and three meta-GGAs (mGGAs) (including dependence on the kinetic energy density or Laplacian). They are PBE[49], a widely used non-empirical functional; revPBE[50], a modified version of PBE that performs well with dispersion corrections in GMTKN55; and BLYP[51,52], an empirical functional combining the Becke88 exchange[51] and Lee-Yang-Parr correlation[52]. We include 4 mGGA functionals: TPSS[53,54], a non-empirical functional designed for broad applicability; SCAN[55], Strongly-Constrained and Appropriately-Normed functional which satisfies all 19 known exact constraints[56]; r^{2}SCAN[57], a numerically stable regularized version of SCAN; and M06L[58], a highly parameterized functional that implicitly captures some dispersion effects.

We also study global hybrids related to these seven. Hybrid functionals incorporate a fraction of exact exchange from HF theory, which helps reduce self-interaction error and improves band gaps. The optimal fraction of exact exchange is around 20-25% for thermochemistry and kinetics.[59] We consider 7 hybrid functionals: PBE0[59,60] (25% exact exchange), B3LYP[61] (20% exact exchange), and hybrid versions of the mGGA functionals with 25% exact exchange (TPSS0[62], SCAN0[63], r^{2}SCAN0[64]), as well as the M06[42] functional with 27% exact exchange.

Databases: To assess the performance and transferability of the D^{2}C-DFT approach, we employ diverse datasets covering a wide range of chemical systems and properties.

Our primary dataset is GMTKN55[33], a comprehensive benchmark suite for general main group thermochemistry, kinetics, and non-covalent interactions. It consists of 55 distinct sub-datasets, totaling 1505 relative energies. We use the weighted total mean absolute deviation (WTMAD-2) metric to evaluate the performance of functionals on this dataset. Each dataset has a weight determined by its average energy divided by the average of all average energies of the 55 databases. Thus, strong bonds have low weights, and non-covalent interactions have high weights. Without this weighting, weak bonds have little effect on any averages. We use this weighting in all analyses of distributions in the database in this paper and refer to W2-GM55 as shorthand for WTMAD-2 on the GMTKN55 database.

The DIET dataset[65] is a smaller version of GMTKN55, designed to accelerate benchmarking while maintaining the diversity of the complete set. It contains 150 relative energies selected using a genetic algorithm, such that the ranking of functionals based on the DIET set closely mimics the ranking based on the complete GMTKN55 set, saving com-

putational costs when finding parameters. For D^{2}C-DFT training, we used the mean absolute error (MAE) of the density-insensitive subset of DIET, considering the varying number of density-insensitive reactions (100-130) for different functionals. However, for the basis set comparison involving the complete DIET set, we employed the WTMAD-2 metric with the original weights from each reaction's home subset, referred to as W2-DIET in this paper. The P30 'poison' dataset [66] is also a subset of GMTKN55, representing the 30 most difficult reactions in it. We used the P30-5 subset, composed of systems up to 5 atoms, to check the impact of the dispersion correction fitting on the most challenging cases.

A specific dataset, the WATER27 [67], will play a vital role, consisting of 27 neutral and charged water clusters with up to 20 molecules. It tests a functional's ability to describe hydrogen bonding and other non-covalent interactions in aqueous systems. Extreme accuracy is vital in this subset for condensed phase simulations of water. [17,21]

Beyond the GMTKN55 dataset, we use four others for validation and testing. The S66×8 dataset [68] is an extended version of the S66 dataset [69] from GMTKN55, providing non-covalent binding energies for 66 small molecular dimers of biological importance at eight different intermolecular distances. This extension allows for a more comprehensive assessment of a functional's ability to describe non-covalent interactions across a range of distances. We used CCSD(T)/CBS energy from Ref. [70].

The Bauzá dataset [71] contains 30 complexes featuring halogen, chalcogen, and pnictogen bonds, which are essential non-covalent interactions. This dataset tests a functional's ability to describe σ-hole interactions and the impact of dispersion corrections on these systems. We used geometries and revised CCSD(T)/CBS values from Ref. [72].

Finally, the S6L [73] and L7 [74] datasets contain large supramolecular complexes, with S6L focusing on host-guest systems and L7 on extended molecular complexes. These datasets test the ability of functionals to capture dispersion interactions in large systems. These are vital as small errors in dispersion corrections are magnified in these larger systems. The S6L is the half of original S12L (2a, 2b, 4a, 5a, 6a, 7b), and we used reference DLPNO-CCSD(T_0)/CBS energy from Ref. [75] for both S6L and L7.

Basis sets: We employed the widely-used Karlsruhe def2 family [76,77] of basis sets throughout this work, with the default being def2-QZVPPD, a large and accurate basis set that provides high-quality results. Polarization functions (P) allow for a better description of the distortion of atomic orbitals in molecules, while diffuse functions (D) improve the description of loosely bound electrons, which are essential for both anions and long-range interactions.

Methods: We compare five DFT methodologies. Self-consistent DFA calculations without any corrections (DFT); self-consistent DFA calculations with D4 model dispersion corrections (DFT-D4) [26,27]; DFA calculations on HF densities (HF-DFT) [78–81]; HF-DFT with dispersion correction

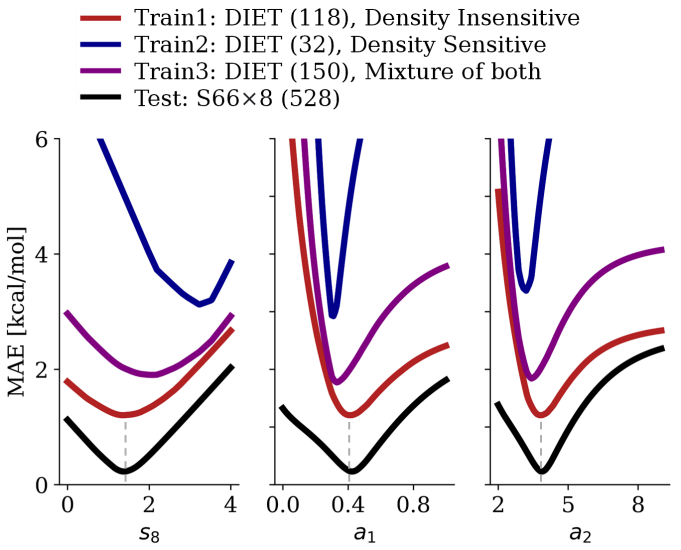

Figure 2: Parameter dependence of various training sets for D^{2}C-B3LYP, showing the effects of individually adjusting each parameter while fixing the others at their optimal values. The dataset size for each set is indicated in parentheses. (See *SI Appendix*, Fig. S1 for r^{2}SCAN.)

using the original D4 parameters for the corresponding self-consistent DFA (HF-DFT-D4$_{\text{orig}}$); and our proposed method, HF-DFT with tailored dispersion correction optimized within the DC-DFT framework (D^{2}C-DFT).

Results and Discussion

Density and Dispersion-Corrected DFT (D²C-DFT)

D^{2}C-DFT employs DFA calculations on HF densities of density-insensitive systems with new dispersion parameters accounting for DC-DFT. An earlier version applied it to the r^{2}SCAN functional (the HF-r^{2}SCAN-DC4 method [21]), but recent work finds inaccuracies when applied to large molecular systems. [34] Given that up to 60 % of interaction energy in large systems can stem solely from dispersion contributions, careful consideration in parameterization becomes crucial. This work aims to refine and expand HF-r^{2}SCAN-DC4, focusing on its parameterization process.

For efficient parameterization, we use the DIET subset. For any specific DFA, we first identify any reactions that are density-sensitive and remove them to ensure density-driven errors have negligible impact on dispersion corrections. The density-sensitive reactions depend on the choice of DFA. Through global optimization using the density-insensitive training set from DIET, we find roughly 30 local minima. We next ranked these local minima based on their W2-GM55 and selected the top 20 parameter sets. These were then re-ranked based on their MAE performance on WATER27 to find the best 10, which ensures very high accuracy for WATER27. In the final stage, each was evaluated on the L7 dataset, which contains large organic complexes and ensures

Table 1: Errors in kcal/mol of DFT, DFT-D4, and D^{2}C-DFT across 14 functionals, using five datasets: GMTKN55, WATER27, Bauzá, L7, and S6L. For the last three, "orig" indicates HF-DFT with dispersion correction using the original D4 parameters for the corresponding self-consistent DFA, where boldface denotes the smaller value (if better by more than 20%).

		GMTKN55[a]			WATER27[b]			Bauzá[b]		L7[b,c]		S6L[b,c]	
		DFT	DFT-D4	D^{2}C	DFT	DFT-D4	D^{2}C	D^{2}C	orig	D^{2}C	orig	D^{2}C	orig
GGA	PBE	13.89	10.12	6.53	2.34	7.58	2.01	0.73	0.65	2.53	2.10	**1.72**	6.07
	revPBE	20.62	8.27	6.03	17.51	3.11	8.07	0.47	0.40	1.26	1.40	4.74	5.33
	BLYP	21.10	9.48	6.60	9.79	2.30	0.99	**0.54**	0.73	**0.81**	2.29	3.45	3.29
mGGA	TPSS	15.69	8.98	6.34	5.11	3.66	1.33	0.95	**0.57**	2.17	**1.12**	3.75	3.89
	SCAN	8.64	7.67	5.37	7.07	8.46	1.16	1.64	**0.93**	**1.14**	2.65	**1.90**	4.74
	r^{2}SCAN	8.66	7.11	5.36	4.24	6.30	0.95	1.11	**0.82**	**1.09**	2.10	**2.26**	4.16
	M06L	8.56	8.53	8.17	1.94	1.24	6.55	0.73	0.72	1.19	1.34	3.06	3.26
Hybrid GGA	PBE0	10.94	6.18	5.42	2.22	4.91	1.24	0.89	**0.68**	**0.62**	1.12	**2.30**	3.12
	revPBE0	16.51	5.26	5.47	14.24	3.77	8.67	0.56	**0.41**	1.24	1.16	3.57	3.52
	B3LYP	16.15	6.15	4.67	5.99	3.02	0.80	0.43	**0.33**	**0.71**	1.49	2.64	**1.69**
Hybrid mGGA	TPSS0	13.06	5.80	5.18	5.59	1.86	2.32	0.90	**0.63**	0.69	0.85	2.35	2.67
	SCAN0	7.59	5.91	5.61	4.76	6.36	1.65	1.57	**0.90**	1.62	**0.87**	1.98	**1.05**
	r^{2}SCAN0	7.65	5.47	5.53	2.76	5.05	1.07	1.23	**0.84**	**0.64**	1.72	**0.77**	2.74
	M06	5.92	5.89	6.37	2.65	1.63	5.03	0.83	0.80	2.49	**1.17**	5.78	**1.75**

[a] W2-GM55
[b] Mean absolute error
[c] Calculated with dual-basis HF-DFT [34] using def2-SVPD/def2-TZVPPD basis set with counterpoise correction [82]

our method's ability to precisely depict dispersion forces even when dominant. The best-performing parameter set on L7, in terms of MAE, was ultimately chosen as the optimal parameter set for D^{2}C-DFT. The final optimized parameter sets for D^{2}C-DFT are available next to the standard choices for DFT-D4 from the literature. (*SI Appendix*, Table S1)

Our study, as illustrated in Fig. 2, emphasizes the critical importance of careful training set selection in parameterization. By comparing the outcomes of parameterization using density-insensitive, density-sensitive cases, and a mixture of both from the DIET dataset, we consistently find that exclusively training with density-insensitive cases leads to more precise parameter minima for the unseen test set. The figure demonstrates that calibrating the empirical parameters solely based on density-insensitive reactions (red) consistently leads to the most accurate parameters, as indicated by the minimum MAE (gray dashed line). In contrast, calibrating parameters using density-sensitive reactions (blue) or a combination of density-sensitive and density-insensitive reactions (purple) results in less accurate parameters due to density-driven errors in the loss function. The conventional parameterization process produces sub-optimal parameters. Despite density-sensitive cases being fewer in number, their higher error rates significantly distort the loss function. This analysis extends to the 30 most challenging reactions in the GMTKN55 dataset, the P30 set. Contrary to expectations, training on these difficult cases did not enhance parameter accuracy, reinforcing the necessity of excluding density-sensitive cases for optimal parameter fitting. (*SI Appendix*, Figs. S2 and S3) A fundamental principle in our DC-DFT approach is that accurate parameterization requires training on only functional error. By adhering to this strategy, D^{2}C-DFT effectively separates both density-driven errors and dispersion portions from functional errors.

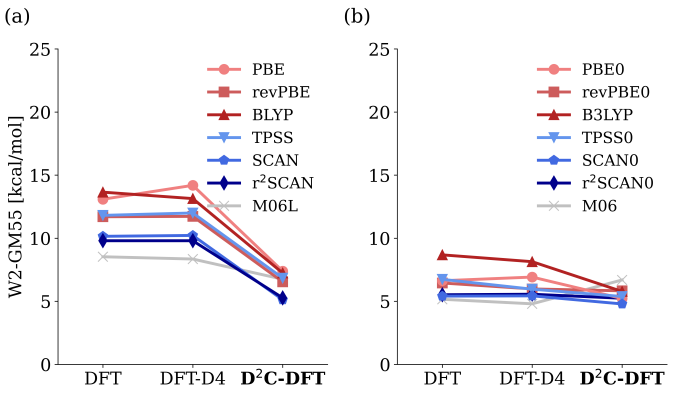

Figure 3: Same as Fig. 1, but including only density-sensitive cases, highlighting the importance of the HF density for semilocal approximations, but less so for hybrids.

Overall performance of D²C-DFT

In Table 1, we report errors for many functionals across several databases. We analyze these fully, reading from the leftmost results to the right. Results for W2-GM55 were already illustrated in Fig. 1, demonstrating a significant error reduction relative to DFT and DFT-D4 for semilocal functionals and the same (but lesser) effect for their global hybrids. If we analyze the individual functionals, we first ignore the Minnesota functionals. Then D^{2}C improves all semilocal functionals over either DFT or DFT-D4, sometimes by a factor of 3. When hybrids

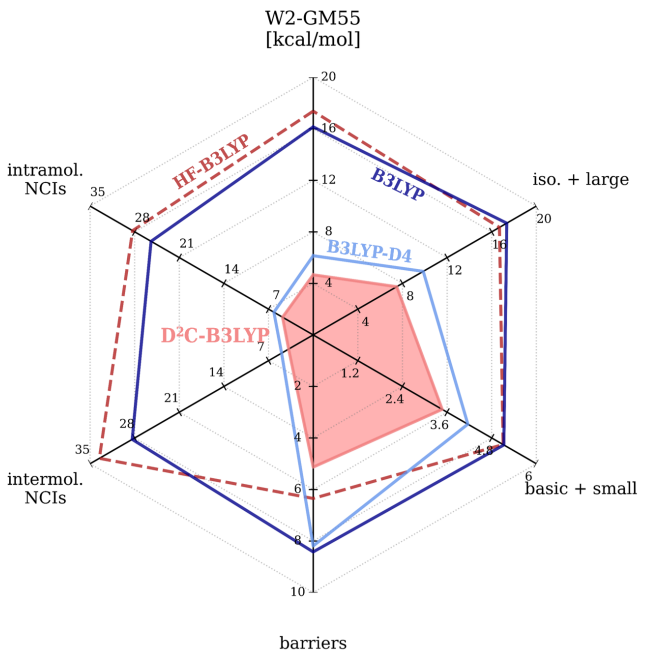

Figure 4: Performance of B3LYP in GMTKN55, divided into standard categories (*SI Appendix*, Tables S2 and S3), for four different methodologies. (See *SI Appendix*, Figs. S4, S5, S6, and S7 for all 14 functionals.)

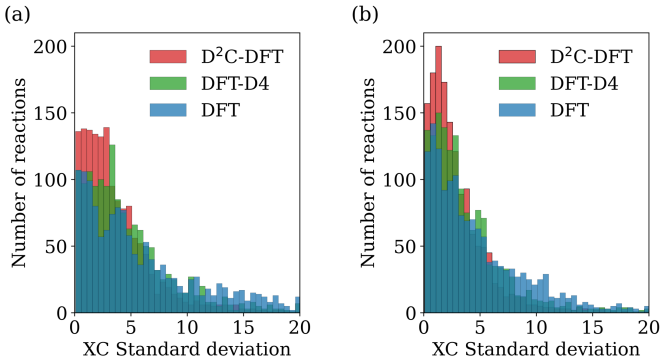

Figure 5: The standard deviation of predictions from (a) six semilocal and (b) six hybrid functionals (no M functionals) for every reaction in GMTKN55. The width of the distribution shrinks from DFT to D^{2}C-DFT, showing improved agreement. For semilocals, the averages are 7.8, 5.4, and 3.8 respectively, with 50%, 40%, and 25% above 5 kcal/mol. The corresponding numbers for hybrids are 5.5, 4, and 3, and 40%, 25%, and 16%, respectively.

are considered, this trend is much weaker. In two cases, results are (very slightly) worsened. We attribute this to the mixing of HF exchange, which likely mixes functional and density-driven errors, which are unaccounted for when choosing the amount of mixing. Figure 3 highlights the performance of D^{2}C-DFT on just density-sensitive reactions, where density-driven errors are significant. The results for density-insensitive reactions, which constitute the majority of the GMTKN55 dataset, exhibit trends similar to those observed in Fig. 1, as they are major in GMTKN55. (*SI Appendix*, Fig. S8)

Finally, we note that, for both Minnesota functionals, almost no effect is seen either in D4 or D^{2}C. We attribute this to their highly parameterized construction, which presumably thoroughly mixes both dispersion and density corrections, leading to no improvement when such effects are systematically accounted for. A critical paper claimed DFT was straying from the exact path due to deficiencies in densities,[83], but DC-DFT found no evidence of errors in chemically significant differences. However, the current analysis (Fig. 1) demonstrates the problems with such approaches.

Focusing on D^{2}C-B3LYP, its superior performance can be attributed to the synergy between the overly repulsive Becke88 exchange[51] and purely attractive dispersion corrections. Radar plots separate the relative performance of methods on different types of GMTKN55 databases. (*SI Appendix*, Tables S2 and S3) Figure 4 showcases this balanced improvement across multiple GMTKN55 subgroups, indicating a harmonious error correction in various chemical systems. Here, we see that HF-B3LYP largely worsens performance in many categories, while D^{2}C-B3LYP outperforms B3LYP-D4 in all categories. Radar plots for all other functionals are available. (*SI Appendix*, Figs. S4, S5, S6, and S7)

Possibly more importantly, we see decreased variation in DFT results, both across different functionals and, for a given functional, across the GMTKN55 database. Figure 5 showcases the first phenomenon, showing the standard deviation among six functionals. Its distribution in GMTKN55 becomes significantly narrower with D^{2}C-DFT, illustrating a notable improvement in precision. Also, by examining the radar plots for all functionals grouped by rung (*SI Appendix*, Figs. S4, S5, S6, and S7), we observe that the D^{2}C variants exhibit pink hexagons of similar size and shape, indicating similar behavior of functionals in the D^{2}C framework.

The second narrowing is for the error distribution within a given functional, as shown in *SI Appendix*, Figs. S9 and S10. This reduced variability among DFA answers can be crucial in real-world situations where a benchmark answer is unavailable.

In *SI Appendix*, we provide all 100k calculations used to generate the W2-GM55 data in this paper. We emphasize that it contains an extraordinary wealth of specific information that can interest specific communities. Some communities care only about one particular functional (such as users of PBE[49] or users of B3LYP[61], largely an orthogonal set). Others might care deeply about performance on a specific type of system, such as non-covalent interactions in general[33] or water in particular[67]. Meanwhile, developers might be most interested in self-interaction errors[33]. The current paper provides only a broad overview and some interesting slices.

To emphasize the importance of looking within data sets, Table 2 gives results for each separate dataset with B3LYP,

Table 2: Performance of B3LYP across the GMTKN55 sub-datasets, with mean absolute errors reported in kcal/mol. The first column (Dens.) indicates whether half or more of the systems in the dataset are density-sensitive by the threshold $\tilde{S} > 2$ (see Eq. 2). The second column (Disp.) indicates whether half or more of the systems in the dataset are dominated by dispersion effects. A system is considered dispersion-dominated if the dispersion-corrected (D4) energy differs from the self-consistent DFT energy by more than 50%. In the majority of cases, D^2C outperforms other methods. (See *SI Appendix*, Table S3 for a description of each dataset.)

	Dens.	Disp.	DFT	DFT-D4	HF-DFT	D^2C-DFT
Basic properties and reaction energies for small systems						
W4-11	YES	NO	3.66	3.16	7.44	5.60
G21EA	NO	NO	2.28	2.31	2.73	2.69
G21IP	NO	NO	3.77	3.74	4.14	4.11
DIPCS10	NO	NO	4.56	4.57	4.19	4.33
PA26	NO	NO	2.29	1.97	1.47	**1.18**
SIE4x4	YES	NO	17.44	17.72	12.46	12.77
ALKBDE10	NO	NO	4.43	4.33	4.48	3.99
YBDE18	NO	YES	8.25	4.72	7.39	**2.62**
AL2X6	NO	YES	8.89	3.23	9.50	2.78
HEAVYSB11	NO	NO	7.57	3.29	7.63	2.71
NBPRC	NO	YES	5.11	2.00	5.76	**1.29**
ALK8	NO	YES	5.82	4.68	6.09	4.61
RC21	YES	YES	2.09	2.43	6.63	3.70
G2RC	NO	NO	2.36	2.57	2.12	2.00
BH76RC	NO	NO	2.03	1.95	1.83	1.57
FH51	NO	YES	3.85	2.51	4.07	2.05
TAUT15	NO	NO	1.15	1.14	0.63	0.69
DC13	NO	NO	15.04	9.46	15.02	7.82
Reaction energies for large systems and isomerisation reactions						
MB16-43	YES	YES	58.04	28.47	64.66	26.45
DARC	NO	NO	15.46	7.62	16.07	**5.60**
RSE43	NO	NO	1.99	1.82	1.62	1.55
BSR36	NO	YES	10.72	2.51	10.93	**1.12**
CDIE20	NO	NO	1.25	1.08	1.03	**0.72**
ISO34	NO	NO	2.26	1.74	2.23	1.40
ISOL24	NO	NO	9.45	5.38	9.18	4.43
C60ISO	YES	NO	2.15	2.63	3.68	3.14
PArel	NO	NO	1.18	1.14	1.01	0.91
Reaction barrier heights						
BH76	YES	NO	4.32	5.04	2.73	2.44
BHPERI	NO	YES	4.35	**1.13**	4.75	2.42
BHDIV10	NO	NO	2.75	3.23	2.16	2.03
INV24	NO	YES	1.88	1.02	1.89	1.10
BHROT27	NO	NO	0.41	0.42	0.34	0.41
PX13	YES	NO	3.51	4.17	**0.98**	2.06
WCPT18	YES	YES	**1.03**	2.06	1.67	1.32
Intermolecular noncovalent interactions						
RG18	NO	YES	0.82	**0.16**	0.89	0.20
ADIM6	NO	YES	4.98	**0.24**	5.32	0.43
S22	NO	YES	3.78	0.42	4.19	**0.28**
S66	NO	YES	3.24	0.30	3.59	0.25
HEAVY28	NO	YES	1.31	0.21	1.48	0.18
WATER27	NO	YES	5.99	3.02	10.71	**0.80**
CARBHB12	NO	YES	0.68	0.64	1.03	**0.38**
PNICO23	NO	YES	1.83	0.31	2.41	**0.20**
HAL59	NO	YES	1.77	0.54	2.49	**0.24**
AHB21	NO	YES	0.87	0.41	1.31	**0.24**
CHB6	NO	YES	1.13	0.96	1.24	1.24
IL16	NO	YES	3.94	**0.33**	4.93	0.41
Intramolecular noncovalent interactions						
IDISP	NO	YES	19.24	5.87	16.95	**1.98**
ICONF	NO	NO	0.59	0.28	0.66	0.31
ACONF	NO	YES	0.95	**0.06**	1.04	0.12
AmiN20x4	NO	YES	0.66	0.20	0.76	0.21
PCONF21	NO	YES	3.80	0.36	3.81	**0.25**
MCONF	NO	YES	2.48	0.26	2.70	0.25
SCONF	NO	YES	0.75	0.31	1.38	**0.20**
UPU23	NO	YES	2.47	0.58	2.56	0.59
BUT14DIOL	NO	NO	0.41	0.46	0.68	**0.26**

highlighting in bold whenever one of the methods is more than 20% better than its nearest rival. We have also listed which datasets are density-sensitive (more than half the reactions are) and which are dispersion dominated (DFT and DFT-D4 errors differ by more than half the DFT error). Clearly, D^2C does best most often, but it is interesting to compare it with DFT-D4, i.e., the standard dispersion methodology without density correction. It is not intuitive why using HF densities does not improve some of these datasets. Doubtless, there are accidental error cancellations between the underlying functional error, the error in the dispersion estimate, and the density-driven error, none of which are driven to zero with our methodology.

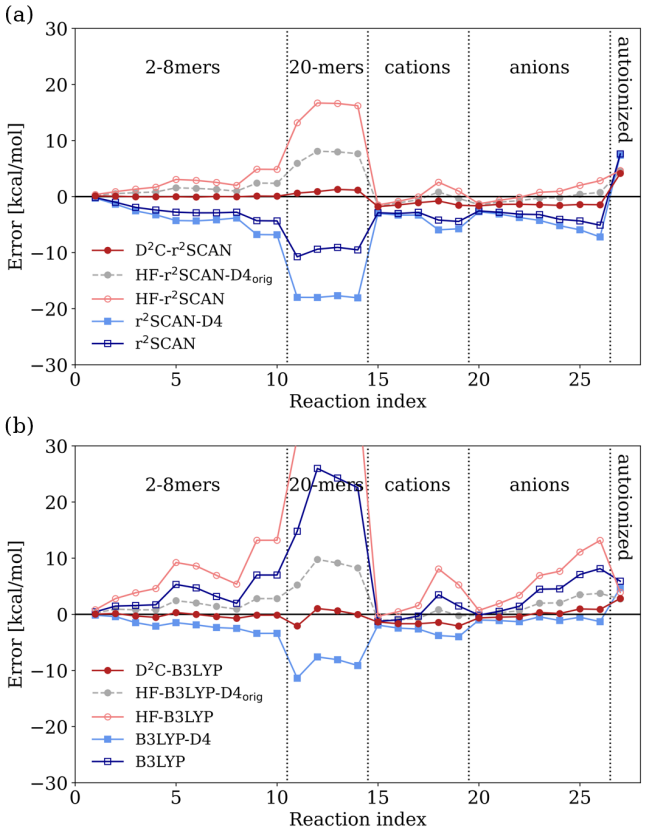

Figure 6: Performance of (a) r^2SCAN and (b) B3LYP functionals on the WATER27 dataset. The D^2C approach outperforms other methods, particularly for larger water clusters. This improvement is crucial for accurately modeling aqueous environments. (See *SI Appendix*, Figs. S11, S12, S13, and S14 for the other functionals.)

The middle columns of Table 1 highlight the outperformance of D^2C on the WATER27 dataset. We regard achieving high accuracy for water clusters as a crucial component of any D^2C methodology. The principle of using HF densities to fix issues in semilocal functionals for water models was first noted by Dasgupta et al.[17,18], and further refinement led to the HF-r^2SCAN-DC4 method[21]. Here, the improvement for the six semilocal functionals is even more considerable than in W2-GM55 and is unpacked for r^2SCAN in Fig. 6(a). Starting from the pure functional, D4 corrections make things worse. Insertion of HF densities significantly overcorrects. Using HF and D4 (original

parameters) gives a better performance, but much better results for the crucial 20-mers occur with D^{2}C. Such a small error is needed for models of water, which is why we use WATER27 as a validation set.

Figure 6(b) shows the corresponding figure for B3LYP, showing the same overall trends and comparable results. A unique observation is the underperformance of D^{2}C-revPBE and D^{2}C-revPBE0 in WATER27. We interpret this as a result of the resolution of charge transfer errors inherent in revPBE family functionals through the use of HF density, eliminating the compensatory error cancellation.[84] WATER27 plots for the remaining functionals are available. (*SI Appendix*, Figs. S11, S12, S13, and S14) This accuracy can also be seen in water hexamer and 20-mers, where D^{2}C-r^{2}SCAN provides the most accurate predictions compared to other dispersion-corrected HF-r^{2}SCAN variants, and getting (almost) all relative energies correct. (*SI Appendix*, Figs. S15 and S16)

The rightmost columns of Table 1 detail D^{2}C-DFT's evaluation across the Bauzá, L7, and S6L datasets. The Bauzá set is analogous to the WATER27 but is not in the validations set. It is discussed in detail in the next section. The rest test the capability of D^{2}C with large molecular structures, as exemplified by S6L and L7.

In summary, our study generalizes the D^{2}C-DFT method from HF-r^{2}SCAN-DC4 across various functionals, achieving a balanced performance in diverse chemical situations. This success stems from the effective use of HF density in mitigating density-driven errors and precise dispersion parameterization within the DC-DFT framework, thus validating the dual-calibration approach's principles and effectiveness.

Origins of density delocalization errors

In this section, we delve into mitigating density-driven errors, which are intrinsically linked to delocalization errors in DFT. Delocalization error remains a major challenge in DFT[85–87], impacting dissociation limits[88], band gaps[89, 90], and charge transfer predictions[91]. Some (but not all) can be alleviated with DC-DFT methods. We use technology developed in Refs. [12] and [15].

A classic (and extreme) case of density delocalization error is stretching an ionic bond to extremes.[92] Figure 7(a) shows conventional DFAs struggling with severe delocalization error in the NaCl dissociation curve, leading to incorrect energies and fractional charges as they approach the dissociation limit. In contrast, D^{2}C-DFT, using HF density, accurately captures the correct charge and densities and thus produces much more accurate energies at the dissociation limit. To demonstrate the underlying reason, we conduct a fractional analysis for infinitely separated Na and Cl atoms, as depicted in Fig. 7(b). While the DFAs exhibit a concave upward curve leading to fractional electron convergence and inaccuracies in dissociation limits (typically about 0.4 of an electron remains transferred, even as $R \to \infty$), HF's concave downward curve has sharp downward cusps exactly at integers, just like the exact curve

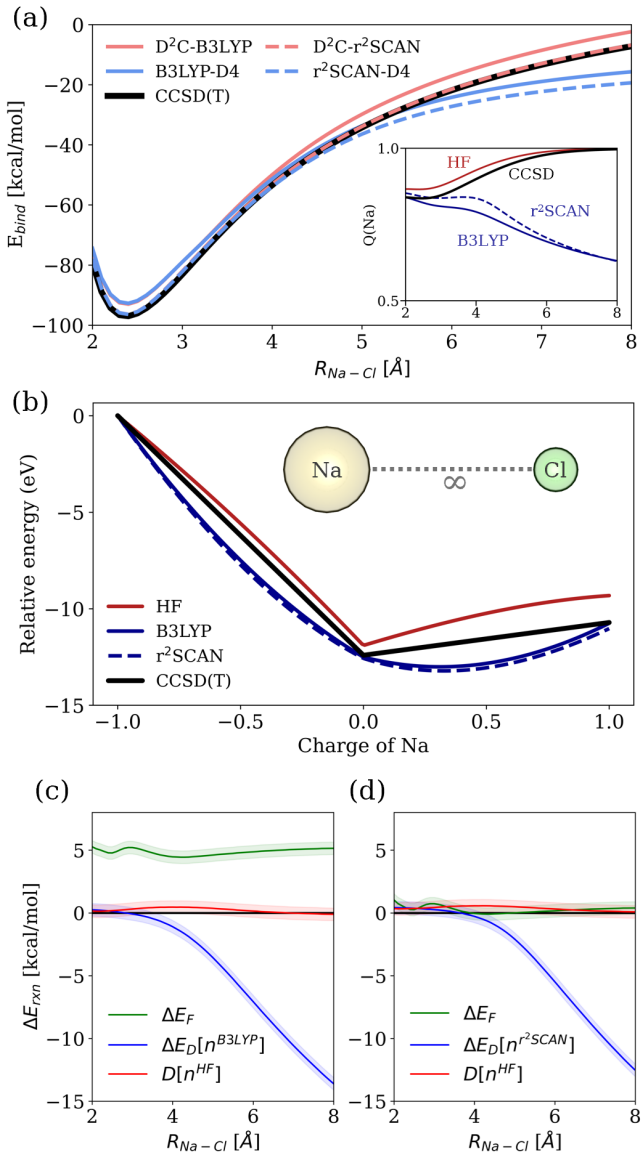

Figure 7: Origin of errors in DFA bond dissociation curves of NaCl: (a) displays the NaCl dissociation curve, with an inset displaying the calculated partial charge on the Na atom; (b) examines fractional electron analysis for isolated Na and Cl with the x-axis indicating charge on Na; (c) and (d) utilize Kohn-Sham inversion to dissect errors within B3LYP and r^{2}SCAN, respectively. The ±0.5 kcal/mol bands illustrate the inversion's uncertainty.[15, 16]

(which consists of linear segments[93]). Note that the HF energies are hopelessly inaccurate, while in the vicinity of the integer, the DFA energies are much more accurate. Hence, the value of HF-DFT, as the HF density and charges remain very accurate, and the functional error of the DFA is very small on the right density.

To gain insights into the remaining error of D^{2}C-B3LYP, we conducted Kohn-Sham inversion[15, 94] as shown in Fig. 7(c), using a reference CCSD density[8], to strictly separate functional and density-driven errors, as in Eq. 1.

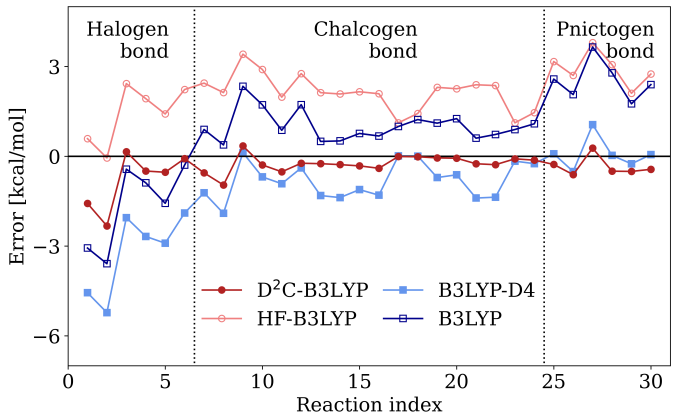

Figure 8: Evaluation of B3LYP behavior using the Bauzá dataset, testing the accuracy of σ-hole interactions. The use of the HF density in D^2C significantly reduces delocalization errors. (See *SI Appendix*, Fig. S17 for r^2SCAN.)

Notably, B3LYP exhibits a constant functional error of approximately 5 kcal/mol, while its density-driven error varies from zero to a significant amount as stretching occurs. In contrast, the density difference of HF remains uniformly close to zero due to its correct behavior. So, the errors in D^2C-B3LYP's dissociation curve in (a) stem from B3LYP's uncorrected functional errors, as D^2C-DFT primarily addresses dispersion errors—a minor component in the NaCl system (∼0.1 kcal/mol). On the other hand, in the case of r^2SCAN illustrated in Fig. 7(d), the density difference of HF and further functional error of r^2SCAN are also nearly zero, which results in D^2C-r^2SCAN's near perfect dissociation curve in (a). Here, r^2SCAN is much better than B3LYP. In either case, the HF density is an excellent proxy for the exact density.

Moving from the illustrative case of NaCl dissociation to the Bauzá dataset, we expand our analysis of delocalization errors. The Bauzá dataset, a collection of Halogen, Chalcogen, and Pnictogen-involved systems, offers an ideal ground to assess the accuracy of σ-hole interaction representation, which is known to pose significant delocalization error,[72] and was attributed to large density-driven errors in our prior work.[14]

As demonstrated in Fig. 8, when dispersion correction is applied to the self-consistent B3LYP, B3LYP-D4 often results in overbinding, worsening results. However, D^2C-B3LYP leads to a remarkable decrease in errors in almost every reaction. Applying the HF density means accurate dispersion is restored in dispersionless situations,[45,95] substantially improves results. This can also be thought of in terms of the absence of self-interaction error in HF.[96] Averages across types are reported in Table 3.

Like the NaCl dissociation case, the effects of delocalization in the self-consistent density in the dissociation of halogen complexes were studied in Ref. [14]. The conventional DFT tends to overbind due to artificial charge transfer. In stark contrast, HF-DFT precisely mirrors the reference curve, adeptly tackling a major element of delocalization error - stretched geometries. This is consistent with other studies that highlight the impressive capability of HF-DFT in mitigating other aspects of delocalization error, including ions-in-solution[11], spin gaps[13], and torsional barriers[16].

Table 3: Mean absolute errors (in kcal/mol) for the Bauzá dataset, categorized by interaction type and overall performance (All).

	Halogen	Chalcogen	Pnictogen	All
B3LYP	1.64	1.02	2.54	1.45
B3LYP-D4	3.22	0.83	0.33	1.21
HF-B3LYP	1.44	2.14	2.93	2.16
D^2C-B3LYP	0.86	0.28	0.43	0.43

Transferability of Parameters across basis sets

For D^2C-DFT applications, we recommend the def2-QZVPPD basis set, quadruple-zeta level with diffusion functions, chosen for its minimal basis set errors. Our parameters were optimized using this set, but this may become unaffordable for large systems. Here, we test the transferability of our dispersion parameters to smaller basis sets, using W2-DIET for efficiency. Figure 9 shows that D^2C-DFT's parameters are transferable effectively down to the triple zeta level with a diffused basis set (def2-TZVPPD) or at the quadruple-zeta level without diffusion functions (def2-QZVP). Below this, performance significantly diminishes. Despite ongoing discussions about the necessity for basis set-specific parameter fitting in dispersion correction,[97,98] we recommend using def2-QZVPPD as the first choice, with feasible applicability down to def2-TZVPPD.

For larger systems, we suggest the dual-basis method[99] for HF-DFT discussed in Ref. [34]. This approach, starting with a double-zeta level calculation, allows a triple- or quadruple-zeta level computation at a much lower computational cost, striking a balance between efficiency and accuracy, which is particularly apt for larger molecules where computational efficiency is paramount.

Conclusion

Our study illustrates the general principle of dual calibration: Separating distinct sources of error when parameters are being fitted in empirical density functionals. Here, the two sources are dispersion corrections and density corrections. By separating these two, we improve results compared to either individually (DFT-D4 for dispersion and HF-DFT for density-correction) or even compared to both if the original D4 parameters are used.

To demonstrate its generality, we applied our procedure to a broad range of non-empirical and only slightly empirical functionals that enjoy considerable popularity in their

	W2-DIET [kcal/mol]						Primitives
basis	**B3LYP**	**B3LYP-D4**	**diff.**	**HF-B3LYP**	**D^{2}C-B3LYP**	**diff.**	
QZVPPD	16.11	6.42	-5%	**16.85**	**4.49**	**-**	1098
QZVP	**15.94**	**6.78**	**-**	16.64	4.66	4%	996
TZVPPD	15.89	6.53	-4%	16.74	4.62	3%	602
TZVP	15.60	8.55	26%	15.73	6.02	34%	356
SVPD	12.54	11.34	67%	13.25	8.80	96%	304
SVP	19.64	18.92	179%	17.19	15.51	245%	202

Figure 9: Transferability of dispersion parameters in B3LYP-D4 and D^{2}C-B3LYP, optimized repectively for the def2-QZVP and def2-QZVPPD, across various basis set sizes within the Karlsruhe (def2-) family. For context, we note the number of primitive Gaussians for the C_8H_{18} molecule. Rows are color-coded based on the difference relative to optimized basis sets (Positive values indicate degraded performance.): Green for <10%, yellow for 10-50%, and red for >50%. This analysis leverages the DIET, a subset of GMTKN55. (See *SI Appendix*, Fig. S18 for r^{2}SCAN.)

respective fields of application. By eliminating density-sensitive cases from our training data, our dispersion corrections differ somewhat from the standard choices, as they correct only functional errors. On the WTMAD-2 measure of the GMTKN55 database, our results are indistinguishable from HF-DFT-D4 using the original parameters. However, because of our DC-DFT training and validation, we do significantly better in crucial cases like WATER27 and large dispersion-dominated databases. Our results here can be considered a generalization of (and improvement over) that of Ref. [21], which applied these principles to the r^{2}SCAN semilocal functional.

While double-hybrid functionals have recently achieved impressive accuracy on GMTKN55, their reliance on costly MP2 calculations limits their applicability to larger systems.[100, 101]. Such functionals suffer much less from dispersion- and density-driven errors, so our dual calibration approach would have a much smaller impact. Nonetheless, given the impressive accuracy that these functionals already achieve, even a much smaller improvement might be significant.

We also point out that the dual calibration approach, perhaps surprisingly, does not rely on the HF density being 'better' (i.e., yielding more accurate energies in approximate functionals) than self-consistent densities, even for density-sensitive problems. The critical step is to find global dispersion parameters (for each approximate functional) on only density-insensitive cases, thereby minimizing any arbitrary bias produced by density-driven errors. The fact that density-sensitive cases can be significantly improved when HF densities are used with dispersion corrections suggests that, at least in those cases, the HF density is better, but only in the sense defined above. Finding a more accurate density than HF density remains a pressing and challenging issue, as it would unveil the true functional errors without making assumptions. Additionally, identifying the various types of functional errors beyond dispersion errors would be required for a clear resolution of them.

In summary, the dual-calibration method, embodied by the D^{2}C-DFT, stands as a promising method with capabilities to improve DFT systematically. The results shown here suggest that some version of this would be helpful in almost all searches for empirical parameters. Its continued development and refinement hold great potential for advancing the DFT functionals and their applications.

Computational Methods

All DFT calculations were performed at Pyscf[102, 103]. Dispersion corrections were facilitated by employing the dftd4 program for D4 corrections[26, 27]. Dispersion parameters of D^{2}C-DFT were optimized using the SciPy[104] shgo optimizer[105]. Results for datasets L7 and S6L were calculated with dual-basis HF-DFT[34, 99] targeting def2-TZVPPD with counterpoise correction[82]. A fractional electron picture was drawn with the method of Refs. [106] and [107]. A Mulliken population analysis[108] based on meta-Lowdin atomic orbitals[109] is used to determine partial charges of NaCl. For the error decomposition, Kohn-Sham inversion was conducted using KS-pies[110], in the Wu-Yang scheme[94], targeting CCSD density[8] at aug-cc-pVTZ basis set[111].

SI Appendix

Dispersion parameters for 14 D^{2}C-DFT and DFT-D4, Abbreviation used for GMTKN55, Description of subsets within GMTKN55, Simplified view on parameterization strategy, Performance on GMTKN55 for 14 functionals, Distribution of weighted errors for 14 functionals across GMTKN55, Performance on WATER27 for 14 functionals, Performance on water hexamers and 20-mers, Evaluation of r^{2}SCAN correction variants using the Báuza dataset, Transferability of dispersion parameters for r^{2}SCAN variants.

Raw data of calculations in GMTKN55 database

Acknowledgement

We are grateful for support from the National Research Foundation of Korea (NRF-2020R1A2C2007468) and Korea Environment Industry & Technology Institute (KEITI) through "Advanced Technology Development Project for Predicting and Preventing Chemical Accidents" Program funded by Korea Ministry of Environment (MOE) (RS-2023-00219144). K.B. acknowledges support from NSF grant No.CHE-2154371. We thank Suhwan Song for the valuable discussions.

Author contributions: M.L., E.S. designed the research; M.L., B.K., and Mingyu Sim performed the calculations; M.L., B.K., Mingyu Sim, Mihira Sogal, Y.K., H.Y., K.B., and E.S. analyzed the data; M.L., K.B., and E.S. wrote the paper.

The authors declare no competing interest.

References

[1] Walter Kohn and Lu Jeu Sham. Self-consistent equations including exchange and correlation effects. *Physical review*, 140(4A):A1133, 1965.

[2] Walter Kohn. Nobel lecture: Electronic structure of matter—wave functions and density functionals. *Reviews of Modern Physics*, 71(5):1253, 1999.

[3] Aurora Pribram-Jones, David A Gross, and Kieron Burke. Dft: A theory full of holes? *Annual review of physical chemistry*, 66:283–304, 2015.

[4] Kieron Burke. Perspective on density functional theory. *The Journal of chemical physics*, 136(15), 2012.

[5] Min-Cheol Kim, Eunji Sim, and Kieron Burke. Understanding and reducing errors in density functional calculations. *Physical review letters*, 111(7):073003, 2013.

[6] Eunji Sim, Suhwan Song, Stefan Vuckovic, and Kieron Burke. Improving results by improving densities: Density-corrected density functional theory. *Journal of the American Chemical Society*, 144(15):6625–6639, 2022.

[7] Stefan Vuckovic, Suhwan Song, John Kozlowski, Eunji Sim, and Kieron Burke. Density functional analysis: The theory of density-corrected dft. *Journal of chemical theory and computation*, 15(12):6636–6646, 2019.

[8] George D Purvis and Rodney J Bartlett. A full coupled-cluster singles and doubles model: The inclusion of disconnected triples. *The Journal of Chemical Physics*, 76(4):1910–1918, 1982.

[9] Krishnan Raghavachari, Gary W Trucks, John A Pople, and Martin Head-Gordon. A fifth-order perturbation comparison of electron correlation theories. *Chemical Physics Letters*, 157(6):479–483, 1989.

[10] Min-Cheol Kim, Eunji Sim, and Kieron Burke. Communication: Avoiding unbound anions in density functional calculations. *The Journal of chemical physics*, 134(17), 2011.

[11] Min-Cheol Kim, Eunji Sim, and Kieron Burke. Ions in solution: Density corrected density functional theory (dc-dft). *The Journal of chemical physics*, 140(18), 2014.

[12] Min-Cheol Kim, Hansol Park, Suyeon Son, Eunji Sim, and Kieron Burke. Improved dft potential energy surfaces via improved densities. *The journal of physical chemistry letters*, 6(19):3802–3807, 2015.

[13] Suhwan Song, Min-Cheol Kim, Eunji Sim, Anouar Benali, Olle Heinonen, and Kieron Burke. Benchmarks and reliable dft results for spin gaps of small ligand fe (ii) complexes. *Journal of chemical theory and computation*, 14(5):2304–2311, 2018.

[14] Yeil Kim, Suhwan Song, Eunji Sim, and Kieron Burke. Halogen and chalcogen binding dominated by density-driven errors. *The journal of physical chemistry letters*, 10(2):295–301, 2018.

[15] Seungsoo Nam, Suhwan Song, Eunji Sim, and Kieron Burke. Measuring density-driven errors using kohn–sham inversion. *Journal of chemical theory and computation*, 16(8):5014–5023, 2020.

[16] Seungsoo Nam, Eunbyol Cho, Eunji Sim, and Kieron Burke. Explaining and fixing dft failures for torsional barriers. *The journal of physical chemistry letters*, 12(11):2796–2804, 2021.

[17] Saswata Dasgupta, Eleftherios Lambros, John P Perdew, and Francesco Paesani. Elevating density functional theory to chemical accuracy for water simulations through a density-corrected many-body formalism. *Nature communications*, 12(1):6359, 2021.

[18] Saswata Dasgupta, Chandra Shahi, Pradeep Bhetwal, John P Perdew, and Francesco Paesani. How good is the density-corrected scan functional for neutral and ionic aqueous systems, and what is so right about the hartree–fock density? *Journal of Chemical Theory and Computation*, 18(8):4745–4761, 2022.

[19] Etienne Palos, Eleftherios Lambros, Saswata Dasgupta, and Francesco Paesani. Density functional theory of water with the machine-learned dm21 functional. *The Journal of Chemical Physics*, 156(16), 2022.

[20] Fabian Belleflamme and Jürg Hutter. Radicals in aqueous solution: assessment of density-corrected scan functional. *Physical Chemistry Chemical Physics*, 25(31):20817–20836, 2023.

[21] Suhwan Song, Stefan Vuckovic, Youngsam Kim, Hayoung Yu, Eunji Sim, and Kieron Burke. Extending density functional theory with near chemical accuracy beyond pure water. *Nature communications*, 14(1):799, 2023.

[22] Bhaskar Rana, Marc P Coons, and John M Herbert. Detection and correction of delocalization errors for electron and hole polarons using density-corrected dft. *The Journal of Physical Chemistry Letters*, 13(23):5275–5284, 2022.

[23] Bhaskar Rana, Gregory JO Beran, and John M Herbert. Correcting π-delocalisation errors in conformational energies using density-corrected dft, with application to crystal polymorphs. *Molecular Physics*, 121(7-8):e2138789, 2023.

[24] Golokesh Santra and Jan ML Martin. What types of chemical problems benefit from density-corrected dft? a probe using an extensive and chemically diverse test suite. *Journal of chemical theory and computation*, 17(3):1368–1379, 2021.

[25] Sándor Kristyán and Péter Pulay. Can (semi) local density functional theory account for the london dispersion forces? *Chemical physics letters*, 229(3):175–180, 1994.

[26] Eike Caldeweyher, Christoph Bannwarth, and Stefan Grimme. Extension of the d3 dispersion coefficient model. *The Journal of chemical physics*, 147(3), 2017.

[27] Eike Caldeweyher, Sebastian Ehlert, Andreas Hansen, Hagen Neugebauer, Sebastian Spicher, Christoph Bannwarth, and Stefan Grimme. A generally applicable atomic-charge dependent london dispersion correction. *The Journal of chemical physics*, 150(15), 2019.

[28] A Otero-De-La-Roza and Erin R Johnson. Non-covalent interactions and thermochemistry using xdm-corrected hybrid and range-separated hybrid density functionals. *The Journal of chemical physics*, 138(20), 2013.

[29] Felix O Kannemann and Axel D Becke. van der waals interactions in density-functional theory: Intermolecular complexes. *Journal of Chemical Theory and Computation*, 6(4):1081–1088, 2010.

[30] Alexandre Tkatchenko, Robert A DiStasio Jr, Roberto Car, and Matthias Scheffler. Accurate and efficient method for many-body van der waals interactions. *Physical review letters*, 108(23):236402, 2012.

[31] Alberto Ambrosetti, Anthony M Reilly, Robert A DiStasio, and Alexandre Tkatchenko. Long-range correlation energy calculated from coupled atomic response functions. *The Journal of chemical physics*, 140(18), 2014.

[32] Suhwan Song, Stefan Vuckovic, Eunji Sim, and Kieron Burke. Density sensitivity of empirical functionals. *The journal of physical chemistry letters*, 12(2):800–807, 2021.

[33] Lars Goerigk, Andreas Hansen, Christoph Bauer, Stephan Ehrlich, Asim Najibi, and Stefan Grimme. A look at the density functional theory zoo with the advanced gmtkn55 database for general main group thermochemistry, kinetics and noncovalent interactions. *Physical Chemistry Chemical Physics*, 19(48):32184–32215, 2017.

[34] Mingyu Sim, Minhyeok Lee, Youngsam Kim, Suhwan Song, Kieron Burke, and Eunji Sim. Extending density-corrected density functional theory to large molecular systems. In preparation, 2024.

[35] Eunji Sim, Suhwan Song, and Kieron Burke. Quantifying density errors in dft. *The journal of physical chemistry letters*, 9(22):6385–6392, 2018.

[36] Carlos Martín-Fernández and Jeremy N Harvey. On the use of normalized metrics for density sensitivity analysis in dft. *The Journal of Physical Chemistry A*, 125(21):4639–4652, 2021.

[37] Daniel Graf and Alex JW Thom. Simple and efficient route toward improved energetics within the framework of density-corrected density functional theory. *Journal of Chemical Theory and Computation*, 19(16):5427–5438, 2023.

[38] Hayoung Yu, Suhwan Song, Seungsoo Nam, Kieron Burke, and Eunji Sim. Density-corrected density functional theory for open shells: How to deal with spin contamination. *The Journal of Physical Chemistry Letters*, 14(41):9230–9237, 2023.

[39] M. Dion, H. Rydberg, E. Schröder, D. C. Langreth, and B. I. Lundqvist. Van der waals density functional for general geometries. *Phys. Rev. Lett.*, 92:246401, Jun 2004.

[40] Kyuho Lee, Éamonn D. Murray, Lingzhu Kong, Bengt I. Lundqvist, and David C. Langreth. Higher-accuracy van der waals density functional. *Phys. Rev. B*, 82:081101, Aug 2010.

[41] Oleg A Vydrov and Troy Van Voorhis. Nonlocal van der waals density functional: The simpler the better. *The Journal of chemical physics*, 133(24), 2010.

[42] Yan Zhao and Donald G Truhlar. The m06 suite of density functionals for main group thermochemistry, thermochemical kinetics, noncovalent interactions, excited states, and transition elements: two new functionals and systematic testing of four m06-class functionals and 12 other functionals. *Theoretical chemistry accounts*, 120:215–241, 2008.

[43] Roberto Peverati and Donald G Truhlar. An improved and broadly accurate local approximation to the exchange–correlation density functional: The mn12-l functional for electronic structure calculations in chemistry and physics. *Physical Chemistry Chemical Physics*, 14(38):13171–13174, 2012.

[44] Lars Goerigk. Treating london-dispersion effects with the latest minnesota density functionals: problems and possible solutions. *The journal of physical chemistry letters*, 6(19):3891–3896, 2015.

[45] Alastair JA Price, Kyle R Bryenton, and Erin R Johnson. Requirements for an accurate dispersion-corrected density functional. *The Journal of Chemical Physics*, 154(23), 2021.

[46] Stefan Grimme, Andreas Hansen, Jan Gerit Brandenburg, and Christoph Bannwarth. Dispersion-corrected mean-field electronic structure methods. *Chemical reviews*, 116(9):5105–5154, 2016.

[47] Axel D Becke and Erin R Johnson. A density-functional model of the dispersion interaction. *The Journal of chemical physics*, 123(15), 2005.

[48] Marvin Friede, Sebastian Ehlert, Stefan Grimme, and Jan-Michael Mewes. Do optimally tuned range-separated hybrid functionals require a reparametrization of the dispersion correction? it depends. *Journal of Chemical Theory and Computation*, 19(22):8097–8107, 2023.

[49] John P Perdew, Kieron Burke, and Matthias Ernzerhof. Generalized gradient approximation made simple. *Physical review letters*, 77(18):3865, 1996.

[50] Yingkai Zhang and Weitao Yang. Comment on "generalized gradient approximation made simple". *Physical Review Letters*, 80(4):890, 1998.

[51] Axel D Becke. Density-functional exchange-energy approximation with correct asymptotic behavior. *Physical review A*, 38(6):3098, 1988.

[52] Chengteh Lee, Weitao Yang, and Robert G Parr. Development of the colle-salvetti correlation-energy formula into a functional of the electron density. *Physical review B*, 37(2):785, 1988.

[53] Jianmin Tao, John P Perdew, Viktor N Staroverov, and Gustavo E Scuseria. Climbing the density functional ladder: Nonempirical meta–generalized gradient approximation designed for molecules and solids. *Physical review letters*, 91(14):146401, 2003.

[54] John P Perdew, Jianmin Tao, Viktor N Staroverov, and Gustavo E Scuseria. Meta-generalized gradient approximation: Explanation of a realistic nonempirical density functional. *The Journal of chemical physics*, 120(15):6898–6911, 2004.

[55] Jianwei Sun, Adrienn Ruzsinszky, and John P Perdew. Strongly constrained and appropriately normed semilocal density functional. *Physical review letters*, 115(3):036402, 2015.

[56] Ryan Pederson and Kieron Burke. The difference between molecules and materials: Reassessing the role of exact conditions in density functional theory. *The Journal of Chemical Physics*, 159(21), 2023.

[57] James W Furness, Aaron D Kaplan, Jinliang Ning, John P Perdew, and Jianwei Sun. Accurate and numerically efficient r2scan meta-generalized gradient approximation. *The journal of physical chemistry letters*, 11(19):8208–8215, 2020.

[58] Yan Zhao and Donald G Truhlar. A new local density functional for main-group thermochemistry, transition metal bonding, thermochemical kinetics, and noncovalent interactions. *The Journal of chemical physics*, 125(19), 2006.

[59] John P Perdew, Matthias Ernzerhof, and Kieron Burke. Rationale for mixing exact exchange with density functional approximations. *The Journal of chemical physics*, 105(22):9982–9985, 1996.

[60] Carlo Adamo and Vincenzo Barone. Toward reliable density functional methods without adjustable parameters: The pbe0 model. *The Journal of chemical physics*, 110(13):6158–6170, 1999.

[61] Philip J Stephens, Frank J Devlin, Cary F Chabalowski, and Michael J Frisch. Ab initio calculation of vibrational absorption and circular dichroism spectra using density functional force fields. *The Journal of physical chemistry*, 98(45):11623–11627, 1994.

[62] Stefan Grimme. Accurate calculation of the heats of formation for large main group compounds with spin-component scaled mp2 methods. *The Journal of Physical Chemistry A*, 109(13):3067–3077, 2005.

[63] Kerwin Hui and Jeng-Da Chai. Scan-based hybrid and double-hybrid density functionals from models without fitted parameters. *The Journal of chemical physics*, 144(4), 2016.

[64] Markus Bursch, Hagen Neugebauer, Sebastian Ehlert, and Stefan Grimme. Dispersion corrected r2scan based global hybrid functionals: r2scanh, r2scan0, and r2scan50. *The Journal of Chemical Physics*, 156(13), 2022.

[65] Tim Gould. 'diet gmtkn55'offers accelerated benchmarking through a representative subset approach. *Physical Chemistry Chemical Physics*, 20(44):27735–27739, 2018.

[66] Tim Gould and Stephen G Dale. Poisoning density functional theory with benchmark sets of difficult systems. *Physical Chemistry Chemical Physics*, 24(11):6398–6403, 2022.

[67] Vyacheslav S Bryantsev, Mamadou S Diallo, Adri CT Van Duin, and William A Goddard III. Evaluation of b3lyp, x3lyp, and m06-class density functionals for predicting the binding energies of neutral, protonated, and deprotonated water clusters. *Journal of Chemical Theory and Computation*, 5(4):1016–1026, 2009.

[68] Jan Rezác, Kevin E Riley, and Pavel Hobza. Extensions of the s66 data set: More accurate interaction energies and angular-displaced nonequilibrium geometries. *Journal of Chemical Theory and Computation*, 7(11):3466–3470, 2011.

[69] Jan Rezác, Kevin E Riley, and Pavel Hobza. S66: A well-balanced database of benchmark interaction energies relevant to biomolecular structures. *Journal of chemical theory and computation*, 7(8):2427–2438, 2011.

[70] Brina Brauer, Manoj K Kesharwani, Sebastian Kozuch, and Jan ML Martin. The s66x8 benchmark for noncovalent interactions revisited: explicitly correlated ab initio methods and density functional theory. *Physical Chemistry Chemical Physics*, 18(31):20905–20925, 2016.

[71] Antonio Bauza, Ibon Alkorta, Antonio Frontera, and Jose Elguero. On the reliability of pure and hybrid dft methods for the evaluation of halogen, chalcogen, and pnicogen bonds involving anionic and neutral electron donors. *Journal of chemical theory and computation*, 9(11):5201–5210, 2013.

[72] A Otero-De-La-Roza, Erin R Johnson, and Gino A DiLabio. Halogen bonding from dispersion-corrected density-functional theory: The role of delocalization error. *Journal of chemical theory and computation*, 10(12):5436–5447, 2014.

[73] Stefan Grimme. Supramolecular binding thermodynamics by dispersion-corrected density functional theory. *Chemistry–A European Journal*, 18(32):9955–9964, 2012.

[74] Robert Sedlak, Tomasz Janowski, Michal Pitonak, Jan Rezac, Peter Pulay, and Pavel Hobza. Accuracy of quantum chemical methods for large noncovalent complexes. *Journal of chemical theory and computation*, 9(8):3364–3374, 2013.

[75] Corentin Villot, Francisco Ballesteros, Danyang Wang, and Ka Un Lao. Coupled cluster benchmarking of large noncovalent complexes in l7 and s12l as well as the c60 dimer, dna–ellipticine, and hiv–indinavir. *The Journal of Physical Chemistry A*, 126(27):4326–4341, 2022.

[76] Florian Weigend and Reinhart Ahlrichs. Balanced basis sets of split valence, triple zeta valence and quadruple zeta valence quality for h to rn: Design and assessment of accuracy. *Physical Chemistry Chemical Physics*, 7(18):3297–3305, 2005.

[77] Florian Weigend. Accurate coulomb-fitting basis sets for h to rn. *Physical chemistry chemical physics*, 8(9):1057–1065, 2006.

[78] Peter MW Gill, Benny G Johnson, John A Pople, and Michael J Frisch. An investigation of the performance of a hybrid of hartree-fock and density functional theory. *International Journal of Quantum Chemistry*, 44(S26):319–331, 1992.

[79] Nevin Oliphant and Rodney J Bartlett. A systematic comparison of molecular properties obtained using hartree–fock, a hybrid hartree–fock density-functional-theory, and coupled-cluster methods. *The Journal of chemical physics*, 100(9):6550–6561, 1994.

[80] Benjamin G Janesko and Gustavo E Scuseria. Hartree–fock orbitals significantly improve the reaction barrier heights predicted by semilocal density functionals. *The Journal of chemical physics*, 128(24), 2008.

[81] Prakash Verma, Ajith Perera, and Rodney J Bartlett. Increasing the applicability of dft i: Non-variational correlation corrections from hartree–fock dft for predicting transition states. *Chemical Physics Letters*, 524:10–15, 2012.

[82] Samuel F Boys and FJMP Bernardi. The calculation of small molecular interactions by the differences of separate total energies. some procedures with reduced errors. *Molecular Physics*, 19(4):553–566, 1970.

[83] Michael G Medvedev, Ivan S Bushmarinov, Jianwei Sun, John P Perdew, and Konstantin A Lyssenko. Density functional theory is straying from the path toward the exact functional. *Science*, 355(6320):49–52, 2017.

[84] Saswata Dasgupta, Etienne Palos, Yuanhui Pan, and Francesco Paesani. Balance between physical interpretability and energetic predictability in widely used dispersion-corrected density functionals. *Journal of Chemical Theory and Computation*, 2023.

[85] Aron J Cohen, Paula Mori-Sánchez, and Weitao Yang. Insights into current limitations of density functional theory. *Science*, 321(5890):792–794, 2008.

[86] Aron J Cohen, Paula Mori-Sánchez, and Weitao Yang. Challenges for density functional theory. *Chemical reviews*, 112(1):289–320, 2012.

[87] Kyle R Bryenton, Adebayo A Adeleke, Stephen G Dale, and Erin R Johnson. Delocalization error: The greatest outstanding challenge in density-functional theory. *Wiley Interdisciplinary Reviews: Computational Molecular Science*, 13(2):e1631, 2023.

[88] Anthony D Dutoi and Martin Head-Gordon. Self-interaction error of local density functionals for alkali–halide dissociation. *Chemical physics letters*, 422(1-3):230–233, 2006.

[89] Aron J Cohen, Paula Mori-Sánchez, and Weitao Yang. Fractional charge perspective on the band gap in density-functional theory. *Physical Review B*, 77(11):115123, 2008.

[90] Paula Mori-Sánchez, Aron J Cohen, and Weitao Yang. Localization and delocalization errors in density functional theory and implications for band-gap prediction. *Physical review letters*, 100(14):146401, 2008.

[91] Stephan N Steinmann, Cyril Piemontesi, Aurore Delachat, and Clemence Corminboeuf. Why are the interaction energies of charge-transfer complexes challenging for dft? *Journal of Chemical Theory and Computation*, 8(5):1629–1640, 2012.

[92] John P Perdew. What do the kohn-sham orbital energies mean? how do atoms dissociate? *Density Functional Methods in Physics*, pages 265–308, 1985.

[93] John P Perdew, Robert G Parr, Mel Levy, and Jose L Balduz Jr. Density-functional theory for fractional particle number: Derivative discontinuities of the energy. *Physical Review Letters*, 49(23):1691, 1982.

[94] Qin Wu and Weitao Yang. A direct optimization method for calculating density functionals and exchange–correlation potentials from electron densities. *The Journal of chemical physics*, 118(6):2498–2509, 2003.

[95] Katarzyna Pernal, Rafal Podeszwa, Konrad Patkowski, and Krzysztof Szalewicz. Dispersionless density functional theory. *Phys. Rev. Lett.*, 103:263201, Dec 2009.

[96] A. Szabo and N.S. Ostlund. *Modern Quantum Chemistry: Introduction to Advanced Electronic Structure Theory*. Dover Books on Chemistry. Dover Publications, 1996.

[97] Erin R Johnson, Alberto Otero-de-la Roza, Stephen G Dale, and Gino A DiLabio. Efficient basis sets for non-covalent interactions in xdm-corrected density-functional theory. *The Journal of Chemical Physics*, 139(21), 2013.

[98] Rebecca Sure, Jan Gerit Brandenburg, and Stefan Grimme. Small atomic orbital basis set first-principles quantum chemical methods for large molecular and periodic systems: A critical analysis of error sources. *ChemistryOpen*, 5(2):94–109, 2016.

[99] Liang and Martin Head-Gordon. Approaching the basis set limit in density functional theory calculations using dual basis sets without diagonalization. *The Journal of Physical Chemistry A*, 108(15):3206–3210, 2004.

[100] Axel D Becke, Golokesh Santra, and Jan ML Martin. A double-hybrid density functional based on good local physics with outstanding performance on the gmtkn55 database. *The Journal of Chemical Physics*, 158(15), 2023.

[101] Axel D Becke. Doubling down on density-functional theory. *The Journal of Chemical Physics*, 159(24), 2023.

[102] Qiming Sun, Timothy C Berkelbach, Nick S Blunt, George H Booth, Sheng Guo, Zhendong Li, Junzi Liu, James D McClain, Elvira R Sayfutyarova, Sandeep Sharma, et al. Pyscf: the python-based simulations of chemistry framework. *Wiley Interdisciplinary Reviews: Computational Molecular Science*, 8(1):e1340, 2018.

[103] Qiming Sun, Xing Zhang, Samragni Banerjee, Peng Bao, Marc Barbry, Nick S Blunt, Nikolay A Bogdanov, George H Booth, Jia Chen, Zhi-Hao Cui, et al. Recent developments in the pyscf program package. *The Journal of chemical physics*, 153(2), 2020.

[104] Pauli Virtanen, Ralf Gommers, Travis E Oliphant, Matt Haberland, Tyler Reddy, David Cournapeau, Evgeni Burovski, Pearu Peterson, Warren Weckesser, Jonathan Bright, et al. Scipy 1.0: fundamental algorithms for scientific computing in python. *Nature methods*, 17(3):261–272, 2020.

[105] Stefan C Endres, Carl Sandrock, and Walter W Focke. A simplicial homology algorithm for lipschitz optimisation. *Journal of Global Optimization*, 72:181–217, 2018.

[106] Erin R Johnson, A Otero-De-La-Roza, and Stephen G Dale. Extreme density-driven delocalization error for a model solvated-electron system. *The Journal of chemical physics*, 139(18), 2013.

[107] Sarah R Whittleton, Xochitl A Sosa Vazquez, Christine M Isborn, and Erin R Johnson. Density-functional errors in ionization potential with increasing system size. *The Journal of chemical physics*, 142(18), 2015.

[108] Robert S Mulliken. Electronic population analysis on lcao–mo molecular wave functions. i. *The Journal of chemical physics*, 23(10):1833–1840, 1955.

[109] Qiming Sun and Garnet Kin-Lic Chan. Exact and optimal quantum mechanics/molecular mechanics boundaries. *Journal of chemical theory and computation*, 10(9):3784–3790, 2014.

[110] Seungsoo Nam, Ryan J McCarty, Hansol Park, and Eunji Sim. Ks-pies: Kohn–sham inversion toolkit. *The Journal of Chemical Physics*, 154(12), 2021.

[111] Thom H Dunning Jr. Gaussian basis sets for use in correlated molecular calculations. i. the atoms boron through neon and hydrogen. *The Journal of chemical physics*, 90(2):1007–1023, 1989.

Supplementary Materials for

Correcting dispersion corrections with density-corrected DFT

MINHYEOK LEE[a], BYEONGJAE KIM[a], MINGYU SIM[a],
MIHIRA SOGAL[b],YOUNGSAM KIM[a], HAYOUNG YU[a],
KIERON BURKE[b], AND EUNJI SIM[a*]

[a]Department of Chemistry, Yonsei University, 50 Yonsei-ro Seodaemun-gu, Seoul 03722, Korea
[b]Department of Chemistry, University of California, Irvine, CA 92697, USA

Table S1: DFT-D4 parameters used in our work. s_6 is set to 1. Refer to Subsection "D^{2}C-DFT" in the main text.

	D^{2}C-DFT				DFT-D4			
	s_8	a_1	a_2	cf.	s_8	a_1	a_2	Ref
PBE	1.78595387	0.88511469	2.32863362	a	0.95948085	0.38574991	4.80688534	[1]
PBE0	1.53360351	0.78689150	3.25641582		1.20065498	0.40085597	5.02928789	[1]
revPBE	1.80966761	0.58558155	2.71965468		1.74676530	0.53634900	3.07261485	[1]
revPBE0	1.74590783	0.40385673	4.26818294		1.57185414	0.38705966	4.11028876	[1]
BLYP	1.65244425	0.56438878	2.65715701		2.34076671	0.44488865	4.09330090	[1]
B3LYP	1.35513689	0.41757850	3.84594813		2.02929367	0.40868035	4.53807137	[1]
TPSS	1.54044984	0.69473318	2.51512802		1.76596355	0.42822303	4.54257102	[1]
TPSS0	1.50843498	0.60162555	3.65500533		1.62438102	0.40329022	4.80537871	[1]
SCAN	1.72616184	0.06450398	8.62911596		1.46126056	0.62930855	6.31284039	[1]
SCAN0	3.69655894	0.16214976	8.90158495		6.1187	0.3750	8.1124	[2]
r^{2}SCAN	0.02734375	0.74707031	3.34667969	b	0.6019	0.5156	5.7734	[3]
r^{2}SCAN0	3.97877459	0.75987648	5.45977445		0.8992	0.4778	5.8779	[3]
M06L	0.75781250	0.81445313	6.16992188		0.59493760	0.71422359	6.35314182	[1]
M06	1.30522230	0.83568617	4.37780185		0.16366729	0.53456413	6.06192174	[1]

[a] Parameters revised from Ref. [4]

[b] Parameters revised from Ref. [5]

*esim@yonsei.ac.kr

Table S2: Abbreviation, description, and the number of reactions included in the GMTKN55[6], classified further by 5 subgroups. In the main text, the Fig. 4 uses this classification.

abbreviation	description	#
GMTKN55	Full GMTKN55	1505
basic + small	Basic properties and reaction energies for small systems	473
iso. + large	Reaction energies for large systems and isomerization reactions	243
barriers	Reaction barrier heights	194
intermol. NCIs	Intermolecular noncovalent interactions	304
intramol. NCIs	Intramolecular noncovalent interactions	291

Table S3: Description of the subsets within the GMTKN55 database. This table is from Ref. [6]. GMTKN55 database is utilized throughout the main text.

Set	Description	#[a]	Weight
	Basic properties and reaction energies for small systems		
W4-11	Total atomisation energies	140 (152)	0.185198
G21EA	Adiabatic electron affinities	25 (50)	1.690459
G21IP	Adiabatic ionisation potentials	36 (71)	0.220644
DIPCS10	Double-ionisation potentials of closed-shell systems	10 (20)	0.086877
PA26	Adiabatic proton affinities (incl. of amino acids)	26 (52)	0.300655
SIE4x4	Self-interaction-error related problems	16 (23)	1.685397
ALKBDE10	Dissociation energies in group-1 and -2 diatomics	10 (20)	0.564505
YBDE18	Bond-dissociation energies in ylides	18 (29)	1.153513
AL2x6	Dimerisation energies of AlX_3 compounds	6 (11)	1.584022
HEAVYSB11	Dissociation energies in heavy-element compounds	11 (22)	0.979616
NBPRC	Oligomerisations and H_2 fragmentations of NH_3/BH_3 systems; H2 activation reactions with PH_3/BH_3 systems	12 (21)	2.051368
ALK8	Dissociation and other reactions of alkaline compounds	8 (17)	0.907969
RC21	Fragmentations and rearrangements in radical cations	21 (41)	1.592221
G2RC	Reaction energies of selected G2/97 systems	25 (47)	1.108788
BH76RC	Reaction energies of the BH76 set	30	2.657109
FH51	Reaction energies in various (in-)organic systems	51 (87)	1.832899
TAUT15	Relative energies in tautomers	15 (25)	18.66054
DC13	13 difficult cases for DFT methods	13 (30)	1.033859
	Reaction energies for large systems and isomerisation reactions		
MB16-43	Decomposition energies of artificial molecules	43 (58)	0.121351
DARC	Reaction energies of Diels–Alder reactions	14 (22)	1.750462
RSE43	Radical-stabilisation energies	43 (88)	7.47666
BSR36	Bond-separation reactions of saturated hydrocarbons	36 (38)	3.509304
CDIE20	Double-bond isomerisation energies in cyclic systems	20 (36)	14.01726
ISO34	Isomerisation energies of small and medium-sized organic molecules	34 (63)	3.901167
ISOL24	Isomerisation energies of large organic molecules	24 (48)	2.593214
C60ISO	Relative energies between C_{60} isomers	9 (10)	0.578511
PArel	Relative energies in protonated isomers	20 (31)	12.27513
	Reaction barrier heights		
BH76	Barrier heights of hydrogen transfer, heavy atom transfer, nucleophilic substitution, unimolecular and association reactions	76 (86)	3.053538
BHPERI	Barrier heights of pericyclic reactions	26 (61)	2.723125
BHDIV10	Diverse reaction barrier heights	10 (20)	1.253833
INV24	Inversion/racemisation barrier heights	24 (48)	1.784849
BHROT27	Barrier heights for rotation around single bonds	27 (40)	9.061109
PX13	Proton-exchange barriers in H_2O, NH_3, and HF clusters	13 (29)	1.703758
WCPT18	Proton-transfer barriers in uncatalysed and water-catalysed reactions	18 (28)	1.624567
	Intermolecular noncovalent interactions		
RG18	Interaction energies in rare-gas complexes	18 (25)	98
ADIM6	Interaction energies of n-alkane dimers	6 (12)	16.92506
S22	Binding energies of noncovalently bound dimers	22 (57)	7.783781
S66	Binding energies of noncovalently bound dimers	66 (198)	10.39698
HEAVY28	Noncovalent interaction energies between heavy element hydrides	28 (38)	45.78596
WATER27	Binding energies in $(H_2O)_n$, $H^+(H_2O)_n$ and $OH^-(H_2O)_n$	27 (30)	0.700517
CARBHB12	Hydrogen-bonded complexes between carbene analogues and H_2O, NH_3, or HCl	12 (36)	9.417873
PNICO23	Interaction energies in pnicogen-containing dimers	23 (69)	13.30064
HAL59	Binding energies in halogenated dimers (incl. halogen bonds)	59 (105)	12.3775
AHB21	Interaction energies in anion–neutral dimers	21 (63)	2.527774
CHB6	Interaction energies in cation–neutral dimers	6 (18)	2.122083
IL16	Interaction energies in anion–cation dimers	16 (48)	0.521253
	Intramolecular noncovalent interactions		
IDISP	Intramolecular dispersion interactions	6 (13)	3.99625
ICONF	Relative energies in conformers of inorganic systems	17 (27)	17.40104
ACONF	Relative energies of alkane conformers	15 (18)	30.99011
AMINO20x4	Relative energies in amino acid conformers	80 (100)	23.30762
PCONF21	Relative energies in tri- and tetrapeptide conformers	18 (21)	35.05036
MCONF	Relative energies in melatonin conformers	51 (52)	11.43436
SCONF	Relative energies of sugar conformers	17 (19)	12.35652
UPU23	Relative energies between RNA-backbone conformers	23 (24)	9.932533
BUT14DIOL	Relative energies in butane-1,4-diol conformers	64 (65)	20.30227

[a] Relative energy counts and required single-point computations (in parenthesis)

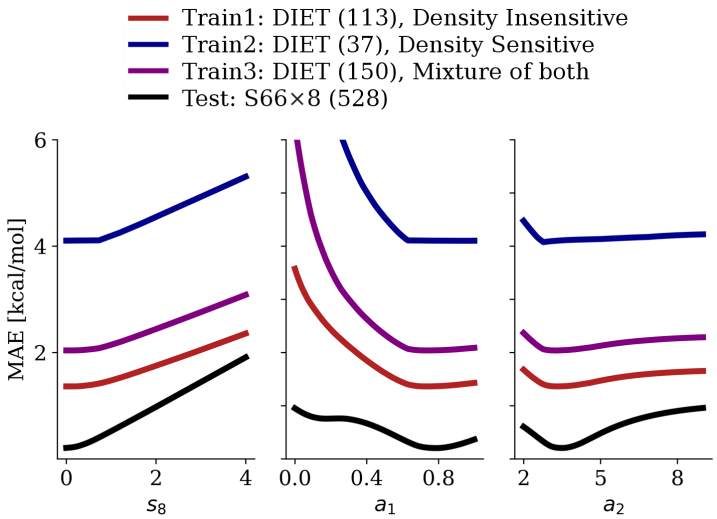

Figure S1: Simplified view on D^{2}C-r^{2}SCAN's parameterization strategy, highlighting the distinction between training set types. Three graphs illustrate the effects of individually adjusting each parameter while fixing the others at optimal values. The datasets utilized in this analysis are from Refs. [7] and [8]. Refer to Fig. 2 in the main text for D^{2}C-B3LYP results.

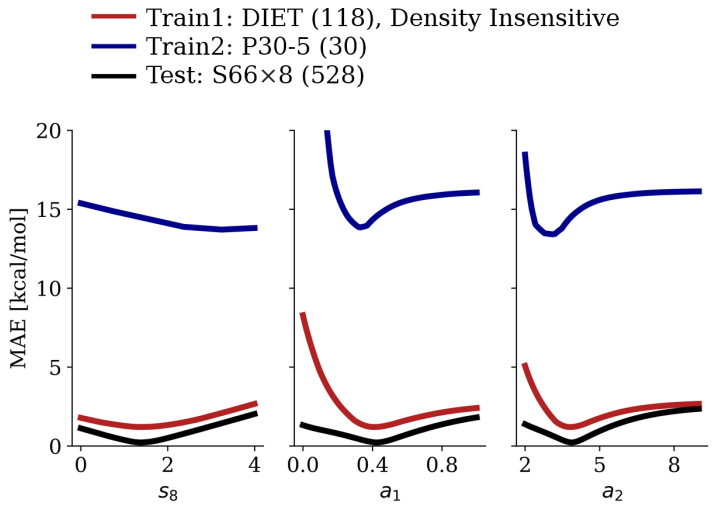

Figure S2: Simplified view on D^{2}C-B3LYP's parameterization strategy, using P30-5 dataset [9] instead, highlighting the distinction between training set types. Refer to Fig. 2 in the main text which utilizes a different training set.

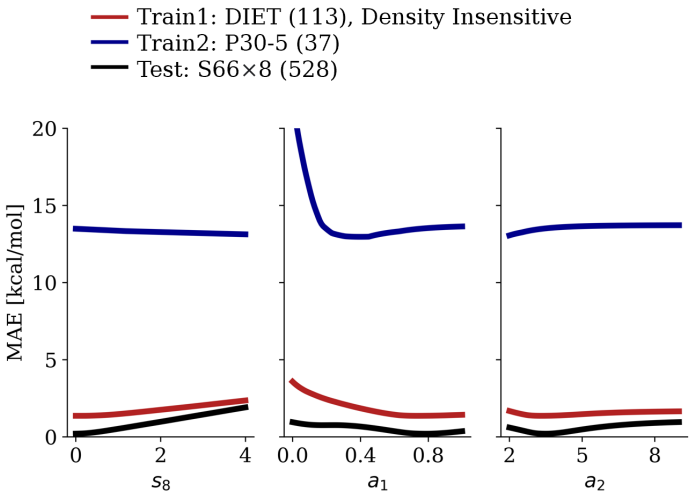

Figure S3: Simplified view on D^{2}C-r^{2}SCAN's parameterization strategy, using P30-5 dataset [9] instead. Refer to Fig. S1 which uses a different training set.

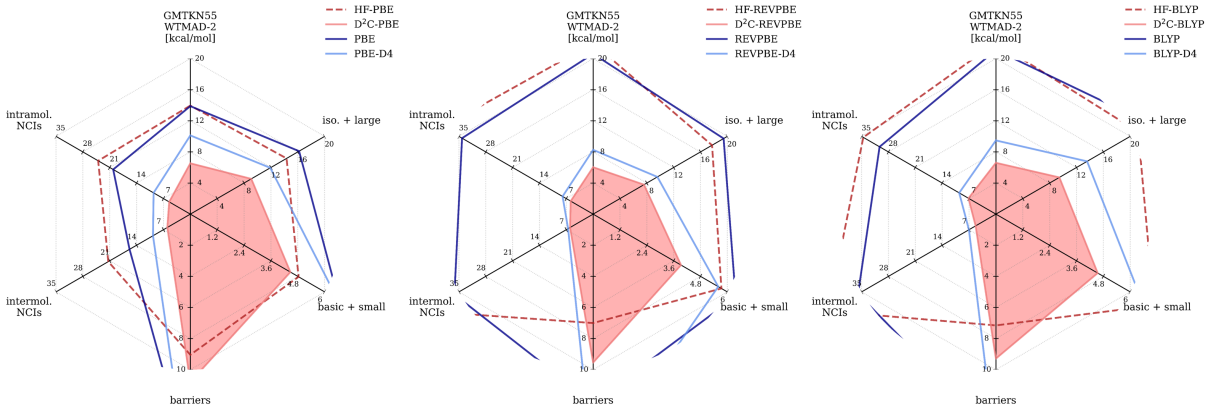

	HF-PBE	D^{2}C-PBE	PBE	PBE-D4
WTMAD-2	13.96	6.53	13.89	10.12
intra. NCIs	24.01	5.5	20.09	9.57
inter. NCIs	21.37	5.99	15.84	9.73
barriers	9.05	10.79	16.34	17.99
basic + small	4.84	4.47	6.63	6.57
iso. + large	14.33	9.08	16.19	11.91

	HF-REVPBE	D^{2}C-REVPBE	REVPBE	REVPBE-D4
WTMAD-2	21.97	6.03	20.62	8.27
intra. NCIs	39.19	5.84	34.18	7.97
inter. NCIs	43.71	6.01	36.17	6.53
barriers	7.0	9.54	12.13	16.32
basic + small	5.73	3.93	6.37	5.59
iso. + large	17.72	7.58	19.44	9.58

	HF-BLYP	D^{2}C-BLYP	BLYP	BLYP-D4
WTMAD-2	22.06	6.6	21.1	9.48
intra. NCIs	34.55	7.15	30.31	9.57
inter. NCIs	43.68	5.28	35.92	7.03
barriers	7.15	9.29	14.17	15.38
basic + small	7.05	4.55	7.74	6.47
iso. + large	21.18	9.45	23.1	13.58

Figure S4: Performance of the GGA functionals variants across the GMTKN55 database. [6] Each section signifies a distinct category. basic + small: Basic properties and reaction energies for small systems, iso + large: Reaction energies for large systems and isomerization reactions, barriers: Reaction barrier heights, intermol NCIs: Intermolecular noncovalent interactions, intramol NCIs: Intramolecular noncovalent interactions, GMTKN55 WTMAD-2: Weighted Total Mean Absolute deviation. Refer to Fig. 4 in the main text for comparison with B3LYP variants.

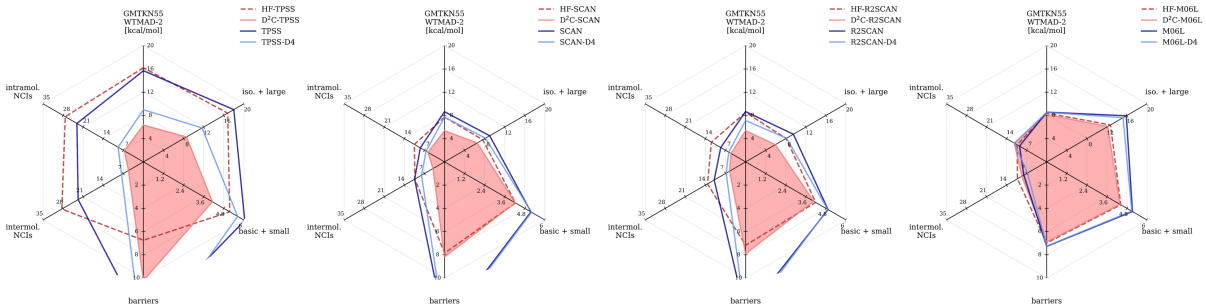

	HF-TPSS	D3C-TPSS	TPSS	TPSS-D4
WTMAD-2	16.21	6.34	15.69	8.98
intra. NCIs	27.23	6.66	23.17	8.82
inter. NCIs	28.44	5.2	22.74	7.61
barriers	6.75	10.23	14.04	16.17
basic + small	5.16	4.12	6.05	5.63
iso. + large	16.78	8.58	18.0	11.68

	HF-SCAN	D3C-SCAN	SCAN	SCAN-D4
WTMAD-2	7.7	5.37	8.64	7.67
intra. NCIs	10.53	5.77	8.44	6.43
inter. NCIs	10.34	4.03	10.44	8.03
barriers	7.86	8.18	14.11	14.37
basic + small	4.24	4.23	5.17	5.21
iso. + large	7.61	6.51	9.0	8.17

	HF-R2SCAN	D3C-R2SCAN	R2SCAN	R2SCAN-D4
WTMAD-2	8.53	5.36	8.66	7.11
intra. NCIs	11.91	5.1	8.66	5.88
inter. NCIs	13.28	5.56	10.95	6.76
barriers	7.18	7.91	13.11	13.57
basic + small	4.19	4.06	4.93	4.9
iso. + large	8.07	5.92	9.52	8.15

	HF-M06L	D3C-M06L	M06L	M06L-D4
WTMAD-2	8.4	8.17	8.56	8.53
intra. NCIs	10.32	11.32	9.49	11.28
inter. NCIs	10.21	8.67	7.99	6.72
barriers	6.98	6.89	7.27	7.25
basic + small	4.43	4.39	5.13	5.09
iso. + large	12.71	12.15	15.87	15.22

Figure S5: Performance of the mGGA functionals variants across the GMTKN55 database.

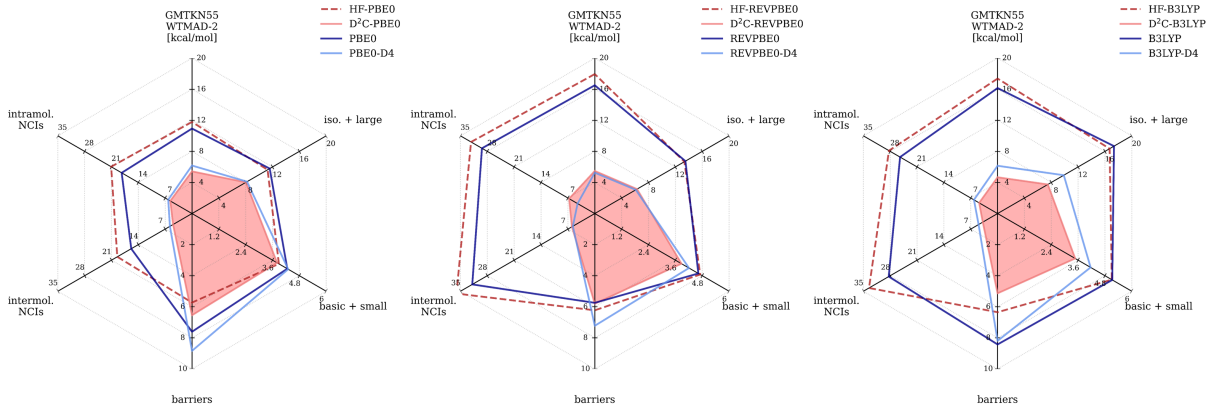

	HF-PBE0	D3C-PBE0	PBE0	PBE0-D4
WTMAD-2	11.79	5.42	10.94	6.18
intra. NCIs	21.09	5.66	18.34	6.2
inter. NCIs	19.48	4.93	15.84	5.76
barriers	5.73	6.54	7.61	8.84
basic + small	3.88	3.8	4.26	4.3
iso. + large	11.26	8.03	11.58	8.21

	HF-REVPBE0	D3C-REVPBE0	REVPBE0	REVPBE0-D4
WTMAD-2	17.95	5.47	16.5	5.26
intra. NCIs	32.24	6.68	29.4	4.48
inter. NCIs	36.04	5.95	31.92	5.71
barriers	6.23	5.8	5.75	7.22
basic + small	4.71	3.87	4.63	4.21
iso. + large	13.34	6.29	13.49	6.1

	HF-B3LYP	D3C-B3LYP	B3LYP	B3LYP-D4
WTMAD-2	17.37	4.67	16.15	6.15
intra. NCIs	28.33	4.81	25.43	6.16
inter. NCIs	33.54	3.85	28.39	4.95
barriers	6.35	5.13	8.42	8.19
basic + small	5.11	3.47	5.13	4.16
iso. + large	16.69	7.49	17.35	9.86

Figure S6: Performance of the Hybrid GGA functionals variants across the GMTKN55 database.

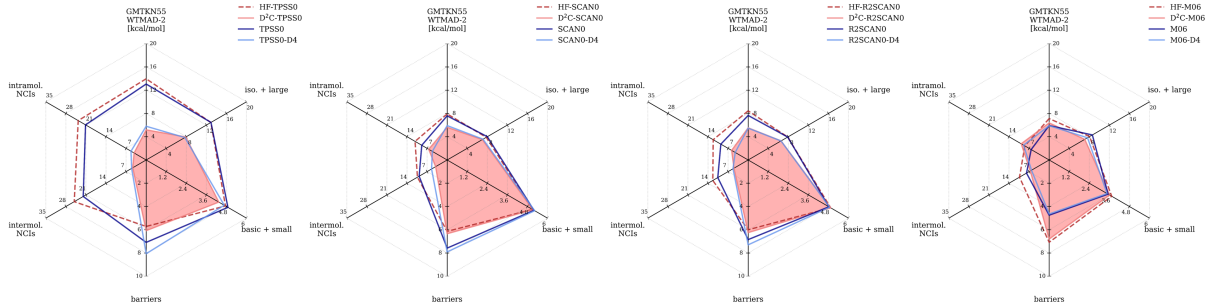

	HF-TPSS0	D3C-TPSS0	TPSS0	TPSS0-D4
WTMAD-2	13.96	5.18	13.06	5.8
intra. NCIs	23.7	4.2	21.14	5.29
inter. NCIs	25.08	4.67	21.95	5.06
barriers	5.71	6.08	7.08	8.06
basic + small	4.74	4.34	4.89	4.67
iso. + large	12.9	7.9	12.92	7.72

	HF-SCAN0	D3C-SCAN0	SCAN0	SCAN0-D4
WTMAD-2	7.91	5.61	7.59	5.91
intra. NCIs	11.2	6.43	8.85	5.17
inter. NCIs	10.37	4.01	9.77	5.43
barriers	6.13	6.34	7.58	7.9
basic + small	5.1	5.13	5.19	5.23
iso. + large	7.8	7.01	8.01	7.15

	HF-R2SCAN0	D3C-R2SCAN0	R2SCAN0	R2SCAN0-D4
WTMAD-2	8.45	5.53	7.65	5.47
intra. NCIs	12.19	5.76	9.53	4.52
inter. NCIs	12.34	4.94	10.59	5.28
barriers	6.0	6.24	6.84	7.29
basic + small	4.94	4.93	4.83	4.87
iso. + large	7.89	6.56	7.88	6.55

	HF-M06	D3C-M06	M06	M06-D4
WTMAD-2	7.12	6.37	5.92	5.89
intra. NCIs	8.47	9.75	6.27	8.91
inter. NCIs	10.35	6.58	7.9	6.15
barriers	7.07	6.8	4.75	4.64
basic + small	3.74	3.61	3.52	3.46
iso. + large	8.06	7.09	8.61	7.64

Figure S7: Performance of the Hybrid mGGA functionals variants across the GMTKN55 database.

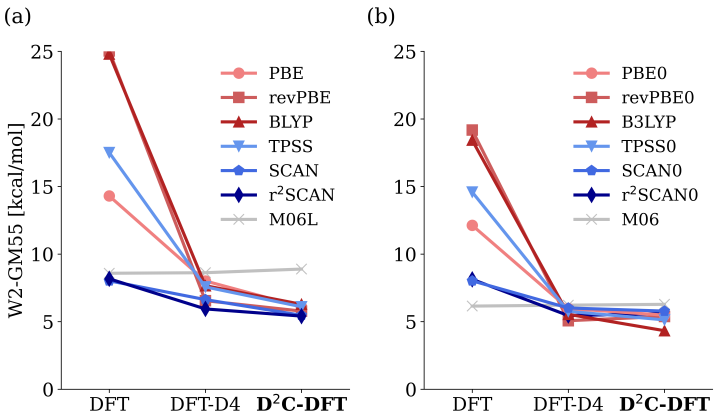

Figure S8: Performance of DFT, DFT-D4, and D^{2}C-DFT on the density-insensitive reactions in GMTKN55 database[6]. See Figs. 1 and 3 in the main text for all reactions in GMTKN55 and only density-sensitive reactions in GMTKN55.

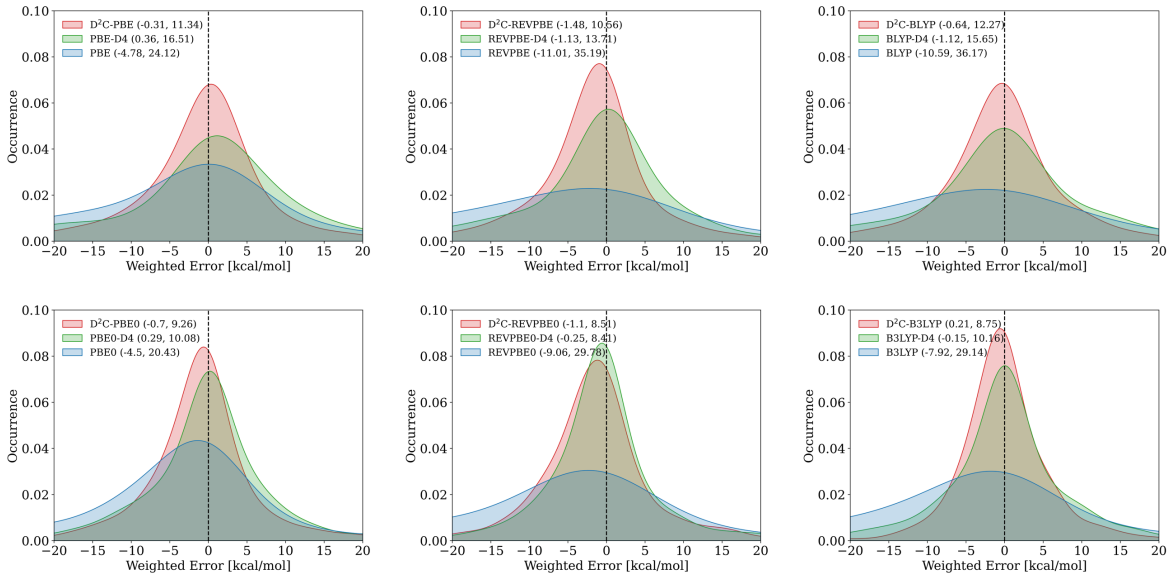

Figure S9: Distribution of Weighted Errors for each GGA-based functionals across 1505 reactions in GMTKN55, including mean and standard deviation (in parenthesis). The reduction in variability is also observed in individual functional with D^{2}C-DFT. Refer to Fig. 5 in the main text to see the standard deviations across functionals.

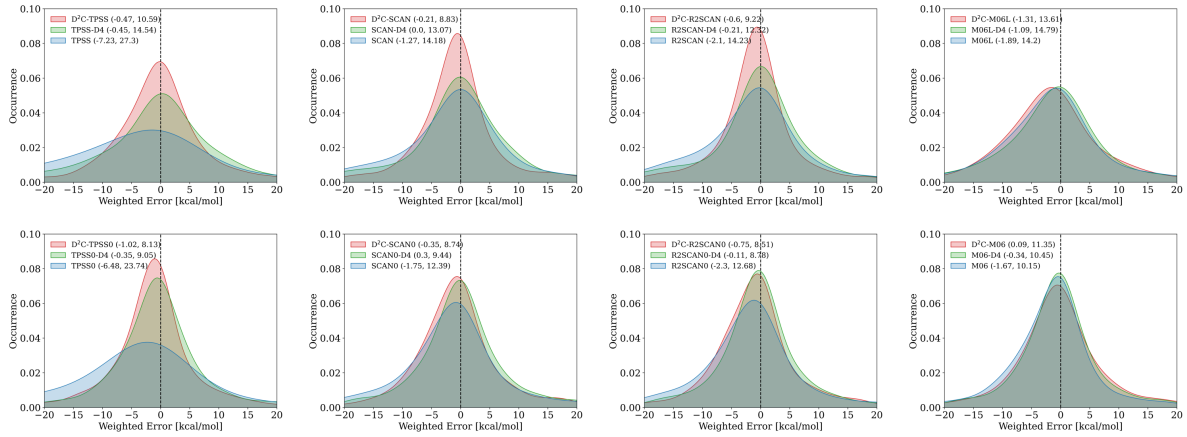

Figure S10: Distribution of Weighted Signed Errors for each mGGA-based functionals across 1505 reactions in GMTKN55, including mean and standard deviation (in parenthesis).

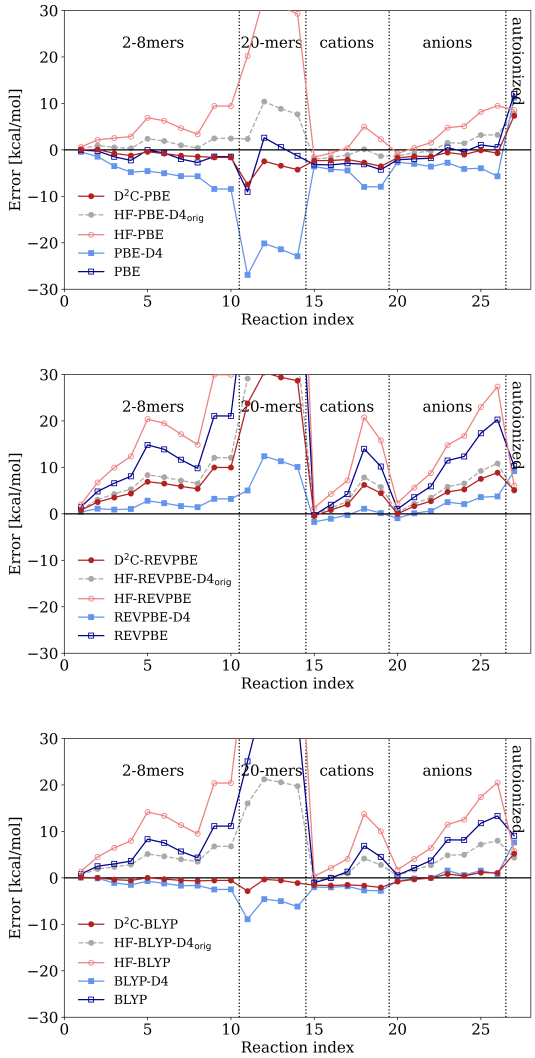

Figure S11: Performance of GGA functionals on WATER27 dataset[10]. To make a negative error implies an overbind effect, the signs of the errors are inverted from the original reference. See Fig. 6 in the main text for the performance on r^{2}SCAN and B3LYP.

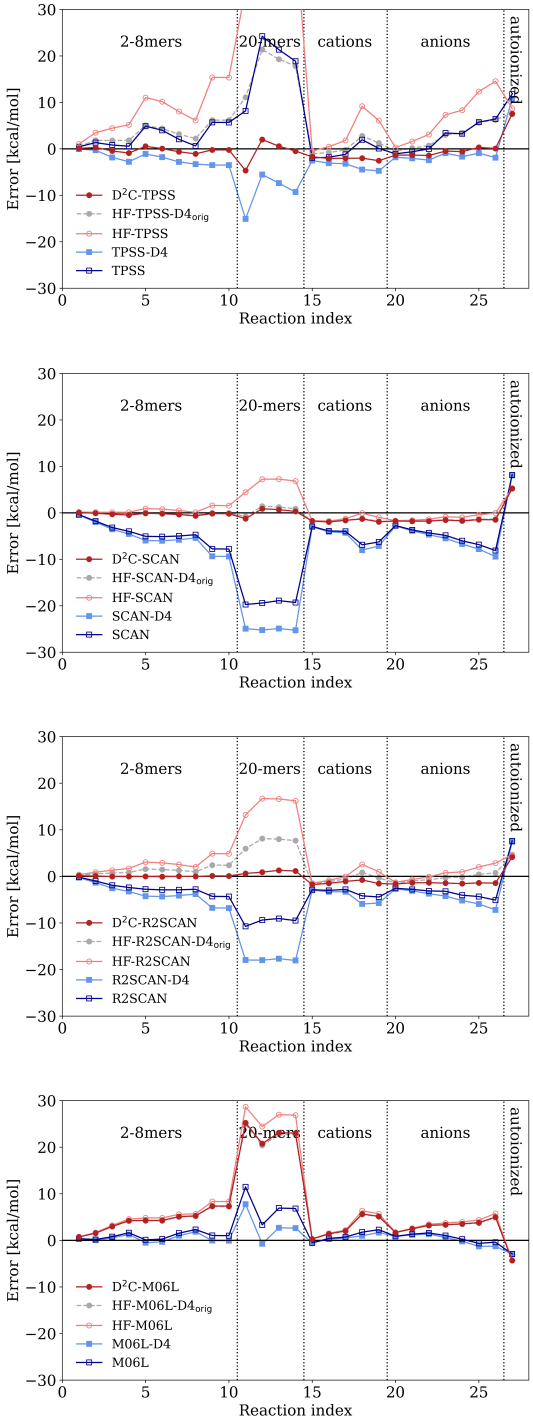

Figure S12: Performance of mGGA functionals on WATER27 dataset.

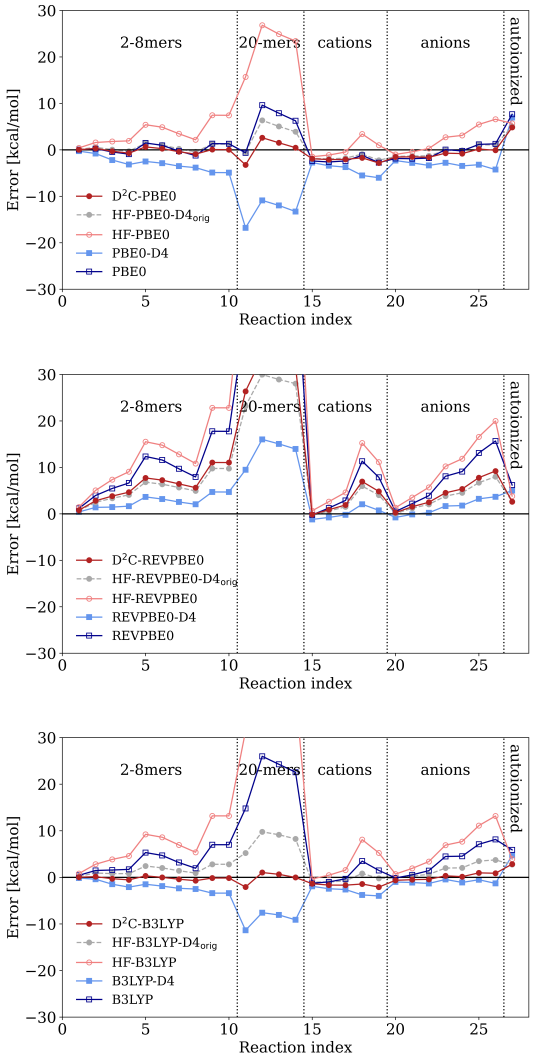

Figure S13: Performance of Hybrid GGA functionals on WATER27 dataset.

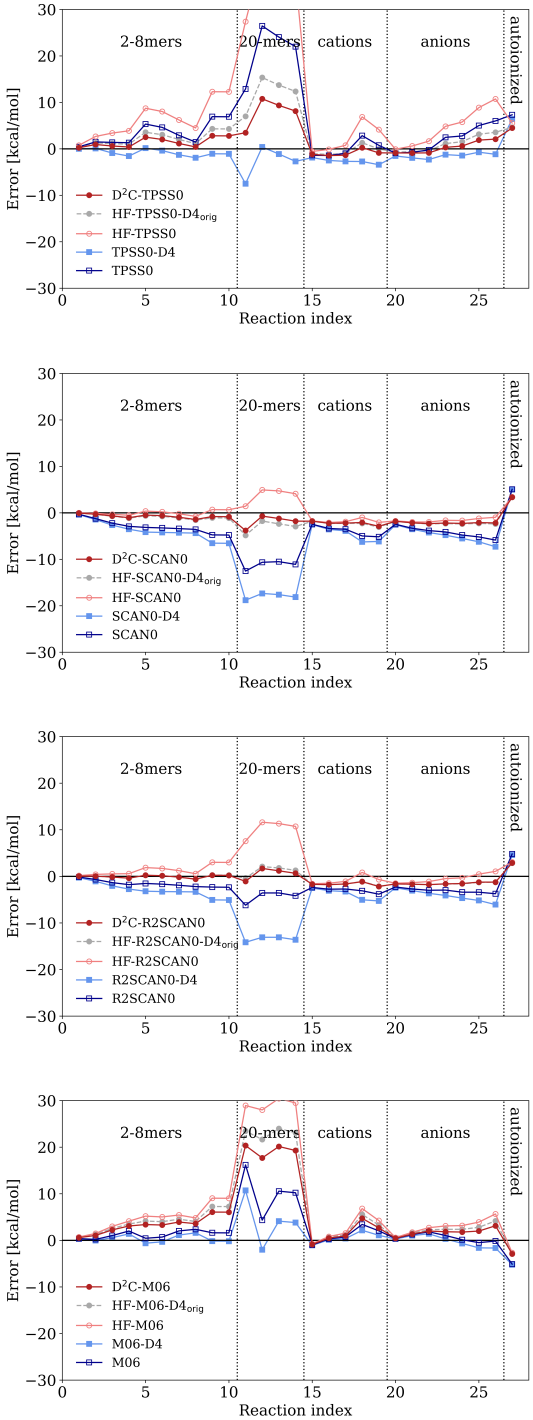

Figure S14: Performance of Hybrid mGGA functionals on WATER27 dataset.

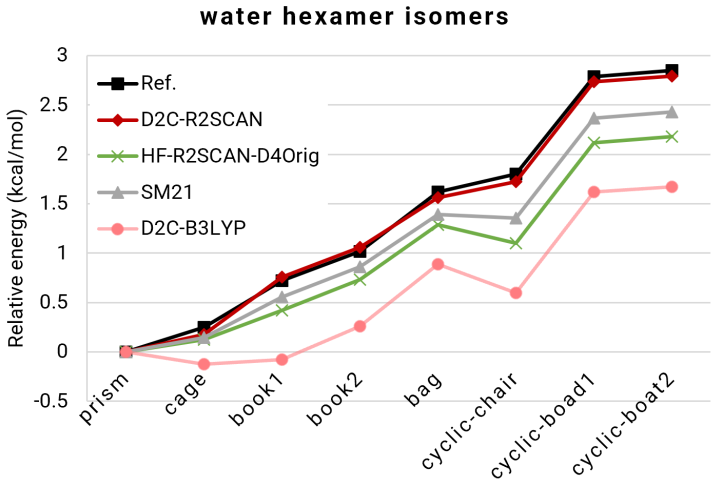

Figure S15: Water hexamers' relative energy compared to prism structure. Geometries are from Ref. [11] and reference CCSD(T)/CBS energy from Ref. [12]. D^2C-r^2SCAN, HF-r^2SCAN-D4Orig, and SM21 are the same HF-r^2SCAN schemes coupled with different dispersion parameters. Dispersion parameter for D4Orig is from Ref. [1] and SM21 is from Ref. [2]. See Subsection 'Overall performance of D^2C-DFT' in the main text.

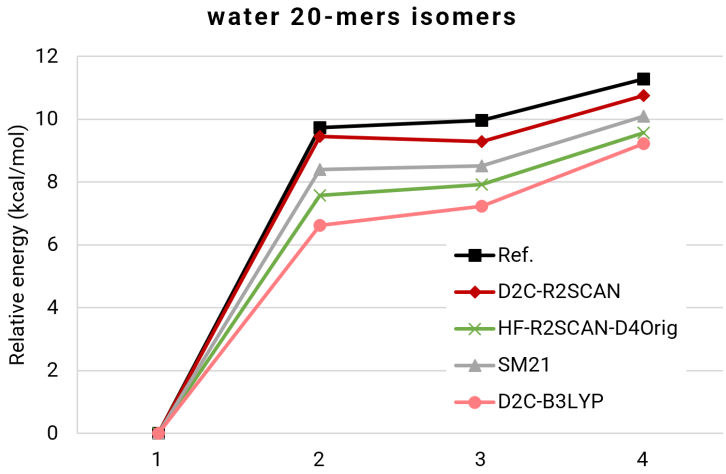

Figure S16: Water 20-mers' relative energies from WATER27[10].

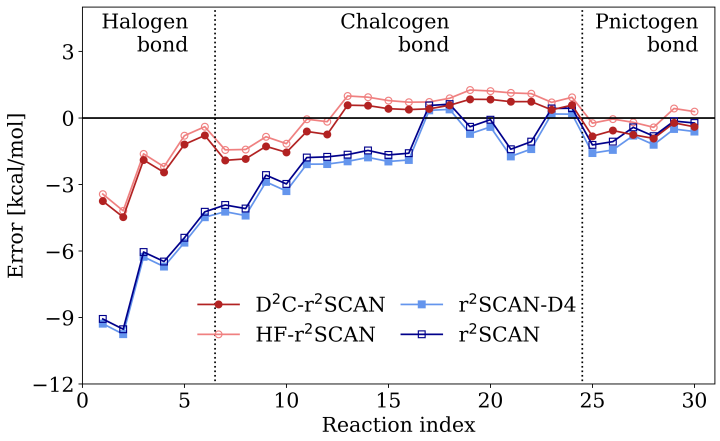

Figure S17: Evaluation of r^{2}SCAN correction variants using the Bauza dataset [13]. This dataset encompasses a wide range of reactions involving Halogen, Chalcogen, and Pnictogen elements, making it an ideal benchmark for testing the accuracy in modeling σ-hole interactions. See Fig. 8 in the main text for the B3LYP results.

	W2-DIET [kcal/mol]						Primitives
basis	**r^{2}SCAN**	**r^{2}SCAN-D4**	**diff.**	**HF-r^{2}SCAN**	**D^{2}C-r^{2}SCAN**	**diff.**	C_8H_{18}
QZVPPD	8.88	7.24	-5%	**7.97**	**4.88**	**-**	1098
QZVP	**9.13**	**7.60**	**-**	7.94	4.98	2%	996
TZVPPD	8.80	7.35	-3%	7.90	4.99	2%	602
TZVP	10.05	8.83	16%	7.63	5.83	19%	356
SVPD	9.77	12.02	58%	6.63	9.16	88%	304
SVP	16.26	17.38	129%	12.52	14.35	194%	202

Figure S18: Transferability of dispersion parameters in r^{2}SCAN-D4 and D^{2}C-r^{2}SCAN, optimized for the def2-QZVP and def2-QZVPPD, across various basis set sizes within the Karlsruhe family[14, 15]. For context, we note the number of primitive Gaussians for the C_8H_{18} molecule. Difference relative to def2-QZVPPD (diff.) is color-coded: Green marks mean degradation below 10 %, yellow for 10-50 %, and red for over 50 %. This analysis leverages the DIET150[8], a subset of GMTKN55[6]. The parameter of D^{2}C-r^{2}SCAN can be safely used down to def2-TZVPPD. See Fig. 9 in the main text for the B3LYP result.

References

[1] Eike Caldeweyher, Sebastian Ehlert, Andreas Hansen, Hagen Neugebauer, Sebastian Spicher, Christoph Bannwarth, and Stefan Grimme. A generally applicable atomic-charge dependent london dispersion correction. *The Journal of chemical physics*, 150(15), 2019.

[2] Golokesh Santra and Jan ML Martin. What types of chemical problems benefit from density-corrected dft? a probe using an extensive and chemically diverse test suite. *Journal of chemical theory and computation*, 17(3):1368–1379, 2021.

[3] Sebastian Ehlert, Uwe Huniar, Jinliang Ning, James W Furness, Jianwei Sun, Aaron D Kaplan, John P Perdew, and Jan Gerit Brandenburg. r2scan-d4: Dispersion corrected meta-generalized gradient approximation for general chemical applications. *The Journal of Chemical Physics*, 154(6), 2021.

[4] Hayoung Yu, Suhwan Song, Seungsoo Nam, Kieron Burke, and Eunji Sim. Density-corrected density functional theory for open shells: How to deal with spin contamination. *The Journal of Physical Chemistry Letters*, 14(41):9230–9237, 2023.

[5] Suhwan Song, Stefan Vuckovic, Youngsam Kim, Hayoung Yu, Eunji Sim, and Kieron Burke. Extending density functional theory with near chemical accuracy beyond pure water. *Nature communications*, 14(1):799, 2023.

[6] Lars Goerigk, Andreas Hansen, Christoph Bauer, Stephan Ehrlich, Asim Najibi, and Stefan Grimme. A look at the density functional theory zoo with the advanced gmtkn55 database for general main group thermochemistry, kinetics and noncovalent interactions. *Physical Chemistry Chemical Physics*, 19(48):32184–32215, 2017.

[7] Jan Rezác, Kevin E Riley, and Pavel Hobza. S66: A well-balanced database of benchmark interaction energies relevant to biomolecular structures. *Journal of chemical theory and computation*, 7(8):2427–2438, 2011.

[8] Tim Gould. 'diet gmtkn55'offers accelerated benchmarking through a representative subset approach. *Physical Chemistry Chemical Physics*, 20(44):27735–27739, 2018.

[9] Tim Gould and Stephen G Dale. Poisoning density functional theory with benchmark sets of difficult systems. *Physical Chemistry Chemical Physics*, 24(11):6398–6403, 2022.

[10] Vyacheslav S Bryantsev, Mamadou S Diallo, Adri CT Van Duin, and William A Goddard III. Evaluation of b3lyp, x3lyp, and m06-class density functionals for predicting the binding energies of neutral, protonated, and deprotonated water clusters. *Journal of Chemical Theory and Computation*, 5(4):1016–1026, 2009.

[11] Sandeep K Reddy, Shelby C Straight, Pushp Bajaj, C Huy Pham, Marc Riera, Daniel R Moberg, Miguel A Morales, Chris Knight, Andreas W Götz, and Francesco Paesani. On the accuracy of the

mb-pol many-body potential for water: Interaction energies, vibrational frequencies, and classical thermodynamic and dynamical properties from clusters to liquid water and ice. *The Journal of chemical physics*, 145(19), 2016.

[12] Desiree M Bates and Gregory S Tschumper. Ccsd (t) complete basis set limit relative energies for low-lying water hexamer structures. *The Journal of Physical Chemistry A*, 113(15):3555–3559, 2009.

[13] Antonio Bauza, Ibon Alkorta, Antonio Frontera, and Jose Elguero. On the reliability of pure and hybrid dft methods for the evaluation of halogen, chalcogen, and pnicogen bonds involving anionic and neutral electron donors. *Journal of chemical theory and computation*, 9(11):5201–5210, 2013.

[14] Florian Weigend and Reinhart Ahlrichs. Balanced basis sets of split valence, triple zeta valence and quadruple zeta valence quality for h to rn: Design and assessment of accuracy. *Physical Chemistry Chemical Physics*, 7(18):3297–3305, 2005.

[15] Florian Weigend. Accurate coulomb-fitting basis sets for h to rn. *Physical chemistry chemical physics*, 8(9):1057–1065, 2006.